

Early cancer detection using deep learning and medical imaging: A survey



Istiak Ahmad ^{a,b,*¹}, Fahad Alqurashi ^{a,2}

^a Department of Computer Science, Faculty of Computing and Information Technology, King Abdulaziz University, Jeddah 21589, Saudi Arabia

^b School of Information and Communication Technology, Griffith University, Queensland 4111, Australia

ARTICLE INFO

Keywords:

Medical imaging
Cancer detection
Classification
Segmentation
Deep learning
Transfer learning

ABSTRACT

Cancer, characterized by the uncontrolled division of abnormal cells that harm body tissues, necessitates early detection for effective treatment. Medical imaging is crucial for identifying various cancers, yet its manual interpretation by radiologists is often subjective, labour-intensive, and time-consuming. Consequently, there is a critical need for an automated decision-making process to enhance cancer detection and diagnosis. Previously, a lot of work was done on surveys of different cancer detection methods, and most of them were focused on specific cancers and limited techniques. This study presents a comprehensive survey of cancer detection methods. It entails a review of 99 research articles collected from the Web of Science, IEEE, and Scopus databases, published between 2020 and 2024. The scope of the study encompasses 12 types of cancer, including breast, cervical, ovarian, prostate, esophageal, liver, pancreatic, colon, lung, oral, brain, and skin cancers. This study discusses different cancer detection techniques, including medical imaging data, image preprocessing, segmentation, feature extraction, deep learning and transfer learning methods, and evaluation metrics. Eventually, we summarised the datasets and techniques with research challenges and limitations. Finally, we provide future directions for enhancing cancer detection techniques.

1. Introduction

Cancer is an assortment of disorders characterized by unregulated cellular proliferation that has the potential to infiltrate and destroy normal tissues. Genetic mutations and environmental triggers cause this condition, potentially impacting many body parts. Over 100 different forms of the condition have already been identified. The condition has a profound influence on people, manifesting in intense physical symptoms such as pain and exhaustion, psychological consequences including stress and despair, and substantial social and financial hardships, including expensive medical expenses and broken relationships. In 2024 (Siegel et al., 2024), the American Cancer Society projects 2001,140 new cancer cases and 611,720 cancer deaths in the United States. Cancer mortality has declined, averting over 4 million deaths since 1991 due to reduced smoking, early detection, and improved treatments, but rising incidence rates for several cancers threaten these gains. From 2015–2019, annual incidence rates increased by 0.6 %–1 % for breast, pancreas, and uterine corpus cancers and by 2 %–3 % for prostate, liver

(in females), kidney, HPV-associated oral cancers, and melanoma. Significant disparities persist, with mortality rates for prostate, stomach, and uterine corpus cancers being double in Black people compared to White people and higher rates for liver, stomach, and kidney cancers in Native American people. GLOBOCAN (Bray et al., 2024) presents global cancer statistics for 2022, reporting nearly 20 million new cases and 9.7 million deaths, with lung cancer being the most diagnosed and leading cause of death. Table 1 lists the major 12 types of cancer statistics from the American Cancer Society (Explore cancer statistics, 2024). The statistics clearly illustrate the importance of early cancer detection system requirements.

Early identification of cancer greatly enhances the likelihood of effective therapy and prolonged survival by detecting the illness at a more controllable phase. This enables the implementation of more efficient and less forceful interventions, resulting in an improved prognosis and higher survival rates. Regular screenings and vigilance about first symptoms are crucial for early cancer detection, eventually improving patient outcomes and lessening the overall impact of the

* Corresponding author at: Department of Computer Science, Faculty of Computing and Information Technology, King Abdulaziz University, Jeddah 21589, Saudi Arabia.

E-mail address: istiak.ahmad@griffithuni.edu.au (I. Ahmad).

¹ 0000-0001-9914-4116

² 0000-0002-7919-747X

disease. Artificial Intelligence (AI) significantly enhanced the smart city concept by improving various sectors, including health, education (Ahmad et al., 2021), transportation (Ahmad et al., 2022a), security (Alqurashi and Ahmad, 2024), and social implications (Ahmad et al., 2022b, Ahmad et al., 2022c). Within healthcare, Computer Aided Diagnosis (CAD) systems assist in early cancer diagnosis by examining medical images using sophisticated algorithms to identify anomalies (Prabhu et al., 2022). They improve screening precision and effectiveness by offering a secondary evaluation, minimizing human mistakes, and rapidly handling substantial data. Furthermore, CAD systems, including machine learning (ML) and deep learning (DL), constantly learn and adapt efficiently to new data and imaging methods that help radiologists make better judgements and enhance cancer treatment. ML algorithms are capable of processing complex datasets and frequently outperform conventional techniques in identifying patterns and abnormalities that may indicate malignant changes. DL is a subset of ML that uses neural networks to evaluate medical images, including MRIs, CT scans, and mammograms, detecting tiny characteristics the human eye would miss. These technologies are crucial because they can handle increasing medical data, lower the risk of incorrect diagnoses, and provide scalable, reliable, and quick solutions for early cancer diagnosis.

1.1. Related work

Table 2 lists the summary of an existing survey or related literature review. While Most of the survey papers focused on machine learning or deep learning algorithms, other important topics like medical imaging, dataset collection, image preprocessing, segmentation, feature extraction, and evaluation metrics were not discussed. Additionally, the article selection process also skips some papers. However, the present study provides a comprehensive discussion of the above topics.

The research questions of this study are listed below:

1. Medical Imaging Data

11. What are the challenges associated with medical imaging data?
12. What preprocessing techniques are used to enhance the data quality?

13. What are the benchmark datasets used for cancer detection?

2. Deep Learning Techniques

21. What are the main deep-learning techniques used in cancer detection?
22. What are the most used algorithms for feature extraction?
23. How can transfer learning be utilized to improve the performance of deep learning models with limited datasets?

3. Discussion and Future Directions

31. What are the challenges and limitations?
32. What are the future directions?

1.2. Aim, novelty and contributions

Previous survey papers have primarily focused on specific types of cancer and limited detection techniques. It covers various techniques, including medical imaging data, image processing, segmentation, feature extraction, deep learning, and transfer learning methods, along with evaluation metrics. This study provides a comprehensive review of cancer detection methods for 12 types of cancer such as breast, cervical, ovarian, prostate, esophageal, liver, pancreatic, colon, lung, oral, brain, and skin cancers.

The aim of this study is to bridge the existing research gap and contribute to improving cancer detection methods. It also raises eight research questions and includes a figure illustrating the systematic workflow of the cancer detection process, from input to output.

The contributions of this study are outlined as follows:

- The study reviews 99 research articles from WoS, IEEE, and Scopus databases published between 2020 and 2024 and discusses their dataset, methods, and output.
- We discuss and summarise the benchmark datasets with data source links, which will enable researchers for further development.
- We discuss various cancer detection techniques and corresponding research studies to provide a comprehensive understanding and practical application of these techniques.
- We also discuss research challenges and limitations with future directions for enhancing cancer detection techniques.

Section 1 discusses the background of the cancer detection approach, related survey paper, research motivation, research questions, and contribution to this paper. Section 2 discusses the article collection process for this study. Section 3 discusses cancer detection techniques, including medical imaging, image processing, deep learning algorithms, transfer learning, and evaluation metrics. Section 4 discusses cancer types by introducing each cancer and corresponding statistics, datasets, and summary for each cancer detection technique. Section 5 discusses the overall summary of the datasets, cancer detection algorithms, research challenges and limitations, and future directions. Section 6 concludes this study by pointing out major aspects of cancer detection techniques using deep learning and medical imaging.

2. Methodology and design

Figure 1 shows the word cloud, which is generated from the articles keywords section. The top 100 keywords are shown in this figure, and the text size is based on the frequency. For example, cancer, learning, breast, detection, feature, imaging, neural, classification, convolutional, etc., are the most commonly used keywords in research articles.

This study collected research articles from the Web of Science (WoS), IEEE, and Scopus. We used the name as a variable in the query, and the

Table 1
Cancer Statistics - 2024 (Explore cancer statistics, 2024).

Cancer	Estimated New Cases			Estimated Deaths		
	Male	Female	Total	Male	Female	Total
Breast	310,720		310,720		42,250	42,250
Cervical		13,820	13,820		4360	4360
Ovarian		19,680	19,680		12,740	12,740
Prostate	299,010		299,010	35,250		35,250
Esoph.	17,690	4680	22,370	12,880	3250	16,130
Liver	28,000	13,630	41,630	19,120	10,720	29,840
Pancre.	34,530	31,910	66,440	27,270	24,480	51,750
Colon	54,210	52,380	106,590	28,700	24,310	53,010
Lung	116,310	118,270	234,580	65,790	59,280	125,070
Oral	41,510	16,940	58,450	8700	3530	12,230
Brain	14,420	10,980	25,400	10,690	8070	18,760
Skin	59,170	41,470	100,640	5430	2680	8290
Total	664,850	634,480	1299,330	213,830	195,670	409,680

Table 2

A comparative analysis of existing survey/literature review.

Ref.	CY	Cancer	MI	Pr	Seg	FE	EM	Models	BD	ASP	NoA	Cha.	FW
Rai (2024)	2024	lung, breast, skin, brain, colorectal, prostate, leukemia		✓		✓		✓	✓		100+	✓	✓
Yaqoob et al. (2023b)	2017–2022 2023	NM		✓	✓	✓		✓	✓	✓	97	✓	✓
Yaqoob et al. (2023a) 2023	NM	NM		✓		✓		✓		✓	117	✓	✓
Murthy and Bethala (2023) 2023	2009–2020	breast, brain, molecular, prostate, prostate, lung, cervical, colon						✓	✓	✓		✓	✓
Sharma et al. (2023) 2023	2012–2023	breast, lung, liver, prostate, brain, skin, colon			✓	✓	✓	✓	✓	✓		✓	✓
Kaur and Garg (2023) 2023	NM	lung, breast, skin, Brain	✓	✓	✓								
Zolfaghari et al. (2023) 2023	2002–2023	breast, prostate, ovarian, leukemia, colon, lung, lymphoma, liver				✓		✓		✓	92	✓	✓
Maurya et al. (2023) 2023	2017–2022	brain, cervical, breast, skin, lung					✓	✓	✓			✓	✓
Kumar et al. (2022) 2021	2009–2021	breast, prostate, liver, brain, stomach, skin				✓	✓			✓	185	✓	✓
Munir et al. (2019) 2019	NM	breast, lung, brain, skin, prostate		✓	✓		✓	✓					
Hu et al. (2018)	2018	breast, lung, skin, prostate, brain, colonial						✓	✓			✓	✓
This Study	2020–2024	breast, cervical, ovarian, prostate, esophageal, liver, colon, lung, oral, skin, brain, pancreatic	✓	✓	✓	✓	✓	✓	✓	✓	120	✓	✓

NM = Not Mentioned, CY = Covered Years, MI = Medical Imaging, Pr = Preprocessing, Seg = segmentation, FE = Feature Extraction, EM = Evaluation Metrics, BD = Benchmark Dataset, AS = Article Selection Process, NoA = Number of Articles, Cha = Challenges, FW = Future Work

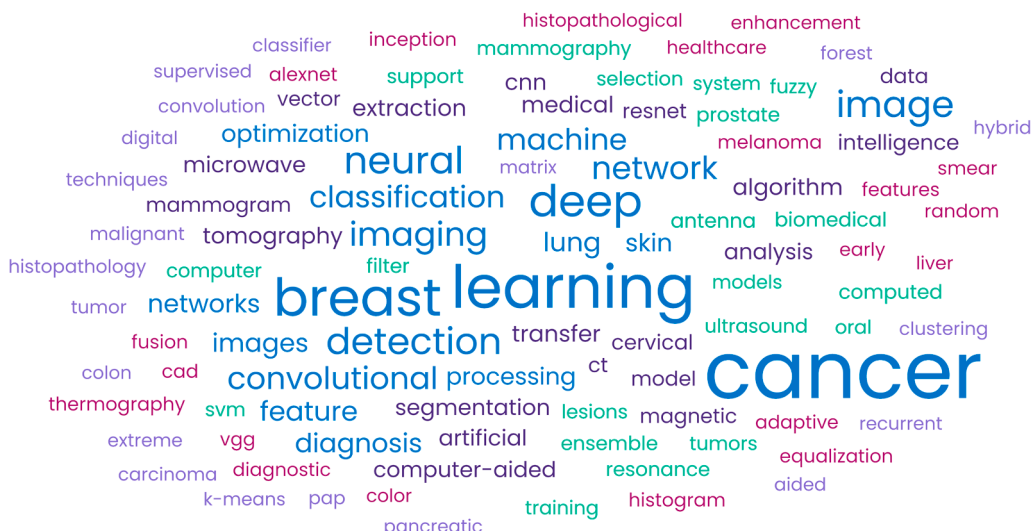


Fig. 1. Word Cloud of 100 Most Used Keywords.

name of the cancer will replace it. The following query was used for WoS to retrieve the articles: (TI=(Name) AND AB=(“image”) AND TI=(“detection”)). Further, we used the following criteria to filter the research articles: article publication duration between 2020 and 2024; document type: article; research areas: engineering, computer science, and medical imaging; language: English; and open access. We applied the following query for IEEE: (“Document Title”: Name) AND (“Abstract”: “image”) AND (“Document Title”: “detection”). The publication duration was from 2020 to 2024, and the documents were only journals. We used the following query for Scopus database: (TITLE(“Name”) AND ABS(“image”) AND TITLE(“detection”)) AND PUBYEAR > 2019 AND PUBYEAR < 2025 AND (LIMIT-TO (SRCTYPE, “j”)) AND (LIMIT-TO (OA, “all”)) AND (LIMIT-TO (SUBJAREA, “COMP”)) AND (LIMIT-TO (DOCTYPE, “ar”)) AND (LIMIT-TO (LANGUAGE, “English”)). Filtering criteria include a subject area: computer science; document type: article; language: English; source type: journal; and open access. Initially, this study collected a total of 444 articles from the three databases. We got

308 articles after removing the duplicate articles. Furthermore, we applied an eligibility check by using a few inclusion and exclusion criteria to finalise the articles. The inclusion criteria include articles using deep learning algorithms for cancer detection and medical imaging and issued in first or second quartiles. The exclusion criteria include review articles and articles published in conferences or in the third and fourth quartiles. Finally, we have reviewed 99 research articles in this study. The article selection process is summarised in [Table 3](#).

3. Cancer detection techniques

Figure 2 provides a detailed analysis of cancer types and the systematic workflow for detecting cancer using medical imaging and deep learning algorithms. The top section classifies cancers by the human body system: reproductive (breast, cervical, ovarian, prostate), digestive (esophageal, liver, pancreatic, colon), respiratory (lung, oral), and others (brain, skin). The bottom section outlines the steps involved in

Table 3
Research Articles Collections.

Cancers	WoS	Scopus	IEEE	Reviewed
Breast	57	120	39	29
Cervical	10	16	3	8
Ovarian	1	2	0	3
Prostate	7	10	6	11
Esophageal	2	3	2	3
Liver	5	8	2	3
Pancreatic	3	5	1	3
Colon	5	7	1	4
Lung	16	39	7	14
Oral	5	5	2	6
Brain	1	3	1	3
Skin	13	32	5	12
Total	125	250	69	142
Total (Initial Identification)				444
Total (Without Duplicate)				308
Total (Reviewed After Eligibility check)				99

cancer detection, starting with medical imaging techniques (see [Section 3.1](#)) such as pathology (histological and cytological) and radiology (X-ray, ultrasound, MRI, CT, PET). Following imaging, the figure describes image preprocessing steps (see [Section 3.2](#)), like re-scaling, normalization, augmentation, noise reduction, and enhancement. Segmentation techniques (see [Section 3.3](#)) like U-NET, watershed transform, and clustering are then utilized, followed by feature extraction methods (see [Section 3.4](#)), including GLCM, HOG, and wavelet transform. Various deep learning algorithms (see [Section 3.5](#)) such as CNNs, RCNNs, RNNs, LSTMs, vision transformers, GANs, and hybrid models are applied, involving transfer learning (see [Section 3.6](#)) with models like YOLO, AlexNet, Inception, DenseNet, ResNet, and VGGNet. The final stage includes evaluation metrics (see [Section 3.7](#)) like accuracy, precision, recall, F1-score, AUC-ROC, specificity, Kappa, and MCC, ensuring the reliability and efficacy of the cancer detection system. This comprehensive overview helps in understanding the integration of advanced imaging and deep learning techniques in cancer detection research.

3.1. Medical imaging techniques

Medical imaging is vital in radiology and pathology and is pivotal in identifying and treating many diseases, including cancer. Radiology ([Kasban et al., 2015](#)) is the field that employs imaging methods to see into the body, whereas pathology is the study of tissues, cells, and organs to identify disorders. Some key techniques in pathology are histopathology, which studies stained tissue sections to recognise disease at the cellular level, and Cytopathology, which studies particular cells from body fluids or fine-needle aspirates. This study focuses on radiology ([Hussain et al., 2022](#)), including key techniques such as X-rays, Computed Tomography (CT) scans, Magnetic Resonance Imaging (MRI), ultrasound, and Positron Emission Tomography (PET) scans.

3.1.1. X-radiation (X-Ray)

X-ray radiography presents numerous advantages, such as being noninvasive, rapid, and painless, which makes it a significant tool for medical and surgical treatment planning and guiding operations like catheter and stent insertions. Nevertheless, it has potential hazards such as exposure to ionizing radiation, which may elevate the probability of getting cancer and induce tissue damage such as cataracts, skin reddening, and hair loss at high levels of radiation. The clinical applications of X-ray radiography are wide-ranging and include chiropractic and dental examinations, projectional radiographs for evaluating fractures and lung diseases, and mammography for breast screening.

3.1.2. Computed tomography Scan (CT)

CT creates comprehensive cross-sectional images of the body using X-rays and computer processing. It is non-invasive, fast, painless, and provides a global view image with high spatial resolution. It can discern minor physical density changes without invasive artery catheter implantation. CT concerns include exposure to ionizing radiation, a lack of real-time information, and difficulties identifying intra-luminal abnormalities. It requires contrast, which may cause allergies and toxicity, and has inferior soft tissue contrast resolution. CT evaluates body components, diagnoses illnesses, injuries, and anomalies, plans and guides

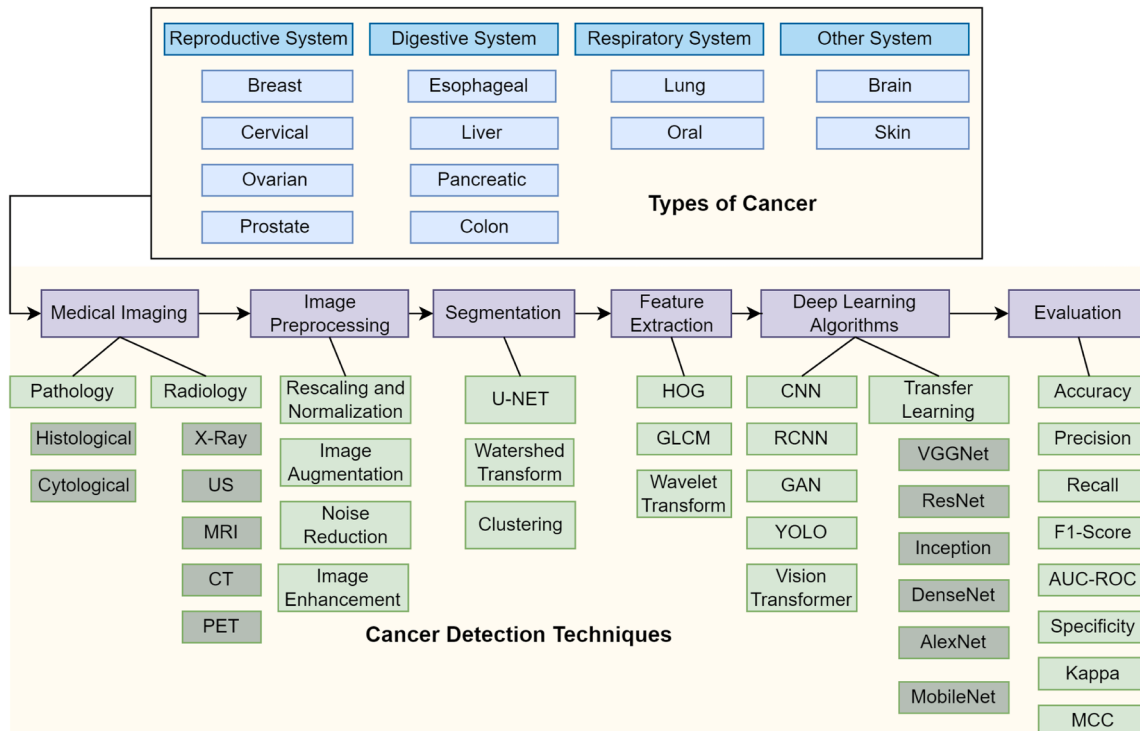


Fig. 2. Systematic Workflow for Cancer Detection.

surgeries, and monitors cancer treatment.

3.1.3. Magnetic resonance imaging (MRI)

MRI generates comprehensive images of bodily tissues using magnetic and radio frequency fields and monitors body chemistry. MRI has several advantages: it is non-invasive, painless, radiation-free, high-resolution, and operator-independent. Its downsides include limited sensitivity, extensive scan and post-processing durations, a large probe need, no real-time information, and difficulties identifying intra-luminal abnormalities. MRI is used to diagnose liver and gastrointestinal disorders, brain and spinal cord abnormalities, tumours, cysts, other abnormalities, joint injuries, pelvic discomfort in women, and unhealthy tissues.

3.1.4. Ultrasonogram (US)

Ultrasonography employs high-frequency sound waves to generate medical images by reflecting off tissues. It detects flow variations and abnormalities within and outside lumens without ionizing radiation, is noninvasive, painless, and provides high-resolution, real-time data. While it lacks defined criteria, is operator-dependent, and is time-consuming, it can monitor fetal growth, imagine head and neck structures, and check solid abdominal organs, including the liver, pancreas, and kidneys, making it useful in cancer diagnosis. This technique helps detect tumours, cysts, and other anomalies, aiding in early cancer detection and surveillance.

3.1.5. Positron emission tomography (PET)

PET employs radiotracers to observe metabolic processes in the body, making it an efficient cancer screening tool. PET scans are noninvasive and give real-time functional information, detecting aberrant metabolic activity linked to cancer. This imaging approach is useful for identifying tiny tumours, determining metastasis, and measuring cancer therapy efficacy. PET scans employ radioactive chemicals and expose patients to ionizing radiation, but their capacity to detect metabolic changes at the cellular level benefits them over CT and MRI, which give structural information. PET/CT improves cancer identification and surveillance by connecting metabolic activity with anatomical features.

3.2. Preprocessing

3.2.1. Gaussian filter

The operation is performed by assembling the image with a Gaussian function, which provides greater weights to pixels closer to the centre of the convolution kernel and lesser weights to those further away. This leads to a phenomenon known as a blurring effect, which reduces the presence of high-frequency noise and small fluctuations in pixel intensity. Gaussian filters are very efficient when decreasing random noise, and preserving edge integrity is crucial. Consequently, they are essential in tasks such as edge recognition, image improvement, and preparing for further analytic stages like segmentation or feature extraction. Equation (1) shows the two-dimensional Gaussian function.

$$\text{Gauss}(x, y) = \frac{1}{2\pi\sigma^2} e^{-\frac{x^2+y^2}{2\sigma^2}} \quad (1)$$

3.2.2. Gabor filter

The Gabor filter (Obayya et al., 2023) is a kind of linear filter that uses a Gabor function as its kernel to collect data on the frequency and direction of local visual elements such as edges and textures. It represents Gaussian envelop modulated by sinusoidal plane wave. Equation (2) shows the Gabor filter (Hammouche et al., 2022), where fr_u is the center frequency, and m , and n denotes the ratio of center frequency and gaussian envelope size. θ_v represents the orientation.

$$\begin{aligned} \delta(x, y) &= \frac{fr_u^2}{\pi mn} e^{\left(\left(\frac{fr_u^2}{m^2}\right)x^2 + \left(\frac{fr_u^2}{n^2}\right)y^2\right)} e^{j2\pi fr_u x'} \\ x' &= x\cos\theta_v + y\sin\theta_v \\ y' &= -x\sin\theta_v + y\cos\theta_v \end{aligned} \quad (2)$$

3.2.3. Median enhanced wiener filter (MEWF)

Alqarafi et al. (2024) implemented MEWF for noise reduction for skin cancer detection. The MEWF technique focuses on the Weiner filter, which transforms the mask matrix pixel values with median values. This effectively reduces the noise in degraded images. The MEWF is shown in Equation (3) (Park et al., 2024), where the mean is replaced with median value; f denotes the degraded image; I_{wf} , and I_{mewf} denote wiener filter and MEWF; θ , and $\bar{\theta}$ represent the mean and median values of the pixels; α , and β represent standard deviation of pixels and noise.

$$\begin{aligned} I_{wf}(x, y) &= \theta + \frac{\alpha^2 - \beta^2}{\alpha^2} (f(x, y) - \theta) \\ I_{mewf}(x, y) &= \bar{\theta} + \frac{\alpha^2 - \beta^2}{\alpha^2} (f(x, y) - \bar{\theta}) \end{aligned} \quad (3)$$

3.2.4. Median filter

The median filter is a non-linear technique that removes noise from visual data. Median filters are often used in CAD because of their capacity to maintain image sharpness, edges, and clarity while minimizing noise.

3.2.5. Bilateral filter

$$BiF[I]_m = \frac{1}{W_m} \sum_{n \in S} G_{as}(|m - n|) * G_{ar}(|I_m - I_n|) * I \quad (4)$$

A bilateral filter is applied to the skin lesion (Midasala et al., 2024) to enhance the image in the spatial domain and improve overall contrast. This filter works on the whole image and enhances the histogram. Adaptive histogram equalization (AHE) differs from bilateral filters by dividing the image into smaller tiles, usually 8×8 pixels. AHE then equalizes the histogram within each tile, improving the visibility of lesion borders. AHE utilizes contrast-limiting techniques to mitigate excessive contrast and noise. The Equation (4) for the bilateral filter has further elements, namely the normalization factor and range weight. In this particular situation, the symbol I is used to represent the input skin lesion image, G_{as} is used to denote the spatial extent of the kernel, and G_{ar} is used to represent the lowest amplitude of an edge. The normalization factor (W_m) ensures that only pixels with intensities identical to the centre pixel are blurred, preserving crisp intensity transitions. This is achieved using the Gaussian space weight ($G_{as}(|m - n|)$) and Gaussian range weight ($G_{ar}(|I_m - I_n|)$).

3.2.6. Entropy filter

The entropy filter represents a statistical metric that quantifies the unpredictability level in an image's pixel values. Equation (5) provides an equation where p is the scaled histogram count for this image (Alzubaidi et al., 2021).

$$\text{Entropy} = - \sum (m \log_2(m)) \quad (5)$$

3.2.7. Other filters

Kavitha et al. (2023) employed an auto-correlogram, Color Layout Filter (CLF), and Binary Pyramid Patterns Filter (BPPF) to remove skin hair from the image for skin cancer detection. Thanh et al. (2020) implemented Adaptive principal curvature to enhance the skin hair contrast more reasonably than the maximum principal curvature and gradient magnitude.

3.2.8. Image augmentation

Data augmentation is essential in diagnosing cancer for several reasons. Addressing the issue of limited annotated medical imaging datasets is critical in medical research, given privacy concerns, the high cost of acquiring and labelling data, and the scarcity of specific cancer categories. Data augmentation is a technique that artificially expands the variety and quantity of the training dataset to minimize overfitting, enhance the model's generalization ability, and improve the accuracy and resilience of DL models. This ensures that the models can identify and categorize malignant tissues, even when confronted with novel and unfamiliar images. Image enhancement methods include changing the shape of an image (such as rotating, scaling, translating, and flipping) and its intensity (by modifying contrast, brightness, and adding noise). They also include more complex techniques such as random cropping, elastic deformations, and creating images using generative adversarial networks (GANs). These strategies replicate many real-world changes in medical images, allowing the models to learn consistent traits and enhance their ability to identify cancer in varied imaging settings and patient groups.

3.3. Segmentation

Image segmentation is the process of splitting an image into separate sections to locate and extract significant elements. Segmentation is vital for accurately demarcating malignancies from healthy tissue using deep learning algorithms like CNN (Li et al., 2018; Sun et al., 2019a; Sun et al., 2019b), which can precisely identify and isolate malignant areas, including tumour size, shape, and location. This capability greatly supports early cancer detection.

3.3.1. U-Net

The U-Net (Ronneberger et al., 2015) is a fully convolutional network (FCN) that was designed for image segmentation. The architecture of U-Net is bidirectional, where the encoder is responsible for extracting significant characteristics, while the decoder is symmetric and growing, facilitating localization by upconvolution. The framework consists of three main components: downsampling, bottlenecking, and upsampling. Every block consists of a convolutional layer, an activation function, and a max pooling function. U-Net doubles the features after each pooling layer to accomplish image segmentation. The upsampling layer of the model consists of a deconvolution layer and an activation function. Due to the fully convolutional nature, the upsampling contains many feature mappings. The absence of completely linked layers in U-Net allows the model to be flexible and capable of processing images of varying sizes.

3.3.2. Watershed transform

The watershed transformation is a region-based technique that represents an image as a topographical map, where bright regions correspond to high altitudes and dark regions correspond to low altitudes. Water is distributed via local low points, where it accumulates in catchment basins and is divided by dams to prevent blending, creating different areas called watersheds. The quantity of segmented objects is contingent upon the quantity of local minima, often resulting in excessive segmentation as a result of a multitude of spurious minima. In order to alleviate this issue, automated markers are used to provide guidance throughout the segmentation process (Sadad et al., 2020).

3.3.3. Kernel fuzzy C-means

Huaping et al. (2021) proposed a kernel-based fuzzy C-means clustering approach for skin cancer image segmentation. They evaluate the distance of the data points from the centre of the cluster using this equation: $kernerFunction = \exp(-\frac{(x-y)^2}{\rho})$. They implemented the following algorithms to get the final clusters: The algorithm started by implementing Kernel Fuzzy C-means to cluster a set of objects and generate a

U membership matrix. The number of closest neighbours t is determined for each pair of elements x_i and x_j . If x_i and x_j are not t closest neighbours, the weight W_{ij} is set to 0. If they are from the same cluster, then W_{ij} is set to 0. Otherwise, W_{ij} is calculated using the following formula: $\exp(\ln 2 \times (u_i \oplus u_j))$, where \oplus denotes the exclusive OR indicating overlap between two fuzzy sets. A diagonal matrix D is then formulated and normalized, where $D_{ij} = \sum_{j=1}^n W_{ij}$. The number of eigenvectors greater than $L = D^{-1/2}WD^{1/2}$ is determined, forming the matrix $P = [p_1, p_2, \dots, p_k]$, which is normalized to create matrix Y. Each row of Y represents a space R^k point, and final clustering is generated (Huaping et al., 2021).

3.4. Feature extraction

The fundamental concept behind feature extraction is to include distinct characteristics that distinguish one input pattern from another pattern to streamline the original data. The pre-processed image separates textural, intensity, and shape features to derive distinctive features. The textual features include contrast, energy, correlation, and homogeneity; intensity features include mean, variance, and standard deviation; and shape features include area, perimeter, and circularity.

3.4.1. Histogram of oriented gradients (HOG)

HOG (Histogram of Oriented Gradients) features are used in computer vision to detect and localize objects by analyzing the differential intensity of local gradients or edge directions. In mammographic images, each region of interest (ROI) is divided into non-overlapping cells, and for each cell, gradients (H_x, H_y) in the x and y directions are calculated (Equation (6)). The magnitude and orientation of these gradients are then computed (Equation (6)), with orientations ranging from -180–180 degrees (signed) or 0–360 degrees (unsigned). Afterwards, the Bin is calculated as the number of Bins multiplied by orientations and divided by 360. Finally, features are computed as a count of the frequency of each value in the image array of Bin using the magnitude as weight.

$$\begin{aligned} H_x &= \frac{d}{dx} f(x, y) \\ H_y &= \frac{d}{dy} f(x, y) \\ \text{magnitude, } |H| &= \sqrt{H_x^2 + H_y^2} \\ \text{orientation, } \theta(x, y) &= \tanh \frac{H_y^2}{H_x^2} \end{aligned} \quad (6)$$

3.4.2. Gray level co-occurrence matrix (GLCM)

The Gray Level Co-occurrence Matrix (GLCM) (Midasala et al., 2024) is a commonly used method in cancer screening to examine the texture of medical images. The GLCM is a statistical technique that quantifies the spatial correlation between pixels. It does this by determining the frequency with which pairs of pixel values occur in a defined spatial connection and organizing these frequencies into a matrix. Various texture properties may be derived from this matrix, including contrast, correlation, homogeneity, and energy (See Equation (7)). The “Contrast” characteristic represents the disparity in intensity between neighbouring pixels. The “Homogeneity” characteristic quantifies the consistency of texture. The term “correlation” quantifies the extent of the linear association between pixels. The term “Energy” represents the level of sharpness and detail in the images. Higher “Energy” levels correspond to more intricate textures. These features present significant insights into the structural formations that dominate the image, which are crucial for identifying between healthy and malignant cells.

$$\begin{aligned}
 \text{Contrast} &= \sum_{x,y=0}^{N-1} S_{x,y}(x - y)^2 \\
 \text{Correlation} &= \sum_{x,y=0}^{N-1} S_{x,y} \left[\frac{(x - \mu_x)(y - \mu_y)}{\sqrt{(\sigma_x^2)(\sigma_y^2)}} \right] \\
 \text{Homogeneity} &= \sum_{x,y=0}^{N-1} \frac{S_{x,y}}{1 + (x - y)^2} \\
 \text{Energy} &= \sqrt{\sum_{x,y=0}^{N-1} S_{x,y}^2}
 \end{aligned} \tag{7}$$

3.4.3. Redundant discrete wavelet transform (RDWT)

The Redundant Discrete Wavelet Transform (RDWT) is an effective method for extracting features in image processing and is very valuable in healthcare fields like cancer diagnosis. RDWT, unlike conventional DWT, does not include down-sampling in the transformation process, therefore maintaining the spatial resolution of the image at various scales. This leads to a representation that is not affected by shifts, which is essential for effectively presenting the intricate characteristics of medical imaging. [Midasala et al. \(2024\)](#) used multilevel feature extraction using GLCM and RDWT for skin cancer detection and classification.

3.4.4. Other feature extraction methods

[Obayya et al. \(2023\)](#) employed GhostNet with AFAO-based hyper-parameter tuning for lung and colon cancer detection. [Alqarafi et al. \(2024\)](#) used a multi-scale Graph Convolution Network (M-GCN) for feature extraction. [Kumar et al. \(2024\)](#) implemented a Spatial Gray-level Dependency Matrix (SGLD) for feature extraction from the brain tumour images.

3.5. Deep learning algorithms

3.5.1. Convolutional neural network

Convolutional Neural Networks (CNNs) ([O'shea and Nash, 2015](#)) are popular for cancer detection and segmentation because they extract useful data and identify patterns. Medical imaging CNN architectures are intended to handle MRI, CT, and histopathology images. Cancer detection CNNs include numerous layers that can independently discern tumour edges, textures, and forms. After these layers, pooling layers reduce spatial dimensions and computational effort while keeping important characteristics. CNNs use fully linked layers with upsampling and skip connections, like the U-Net architecture, to accurately distinguish malignant areas. Training on annotated medical datasets allows these networks to discriminate between benign and malignant tissues. CNNs can precisely find and classify tumours, improving cancer diagnosis, treatment planning, and disease progression. Automatic hyper-parameter tuning algorithms, such as Grey Wolf Optimization (GWO) ([Mohakud and Dash, 2022](#)), Particle Swarm Optimization (PSO), Genetic Algorithm (GA), and Chimp Optimization Algorithm (COA) ([Marzouk et al., 2022](#)), are used to optimize CNN hyper-parameters. Hybrid optimization algorithms, like PSOBER ([Myriam et al., 2023](#)), which is a combination of PSO and Al-Biruni Earth Radius (BER) algorithms, can be used for CNN optimization. [Lu et al. \(2021\)](#) proposed metaheuristic optimization (i.e., marine predators algorithm(MPA)) with CNN to enhance the accuracy of lung cancer detection.

3.5.2. Regional CNN

Regional Convolutional Neural Networks (R-CNNs) are sophisticated CNN designs designed to identify and segment an object's specific regions of interest (ROIs). The original R-CNN employs selective search to generate region suggestions, which are then processed by a CNN to extract features. Subsequently, machine learning algorithms are used for

classification. Fast R-CNN ([Girshick, 2015](#)) enhances speed by using an ROI pooling layer to analyze the full image simultaneously. Faster R-CNN ([Ren et al., 2015](#)) incorporates a Region Proposal Network (RPN) to produce proposals directly from feature maps, enhancing efficiency. Mask R-CNN ([He et al., 2017](#)) enhances Faster R-CNN by including an additional component that predicts segmentation masks, enabling accurate tumour segmentation. The R-CNN versions are very efficient in detecting cancer and accurately identifying and localizing tumours using different imaging techniques. This improves diagnostic precision and aids in focused treatment planning.

3.5.3. YOLO

YOLO (You Only Look Once) ([Ragab et al., 2024](#)) is a real-time object identification architecture that has shown its efficacy in cancer diagnosis in medical imaging due to its rapidity and precision. YOLO approaches object recognition as a singular regression task, directly predicting bounding boxes and class likelihoods for objects inside the whole picture in a single iteration. This single-stage design, including multiple convolutional layers, simultaneously processes the whole image, significantly reducing computation time compared to conventional multi-stage approaches. The image is partitioned into a grid by the architecture, where each grid cell has the task of predicting a certain number of bounding boxes, confidence scores, and class probabilities. Due to its high efficiency and real-time object detection capabilities, YOLO is well-suited for rapidly evaluating large collections of medical images.

3.5.4. Generative adversarial networks

Generative Adversarial Networks (GANs) ([Goodfellow et al., 2020](#)) include two neural networks: the generator and the discriminator. The generator generates artificial data samples, while the discriminator assesses these samples to differentiate between authentic and generated data. The adversarial process facilitates the enhancement of the generator's outputs to the point where they become indistinguishable from authentic data. GANs are crucial for cancer diagnosis because of their capacity to generate synthetic medical imaging of superior quality. These images may be used to enhance the accuracy of training datasets and diagnostic models. GANs possess a structural design that allows them to learn about intricate patterns in data distributions. This ability makes them very efficient in producing lifelike tumour images, which may then be used to enhance the precision of CNNs in identifying and isolating malignant areas. In addition, GANs may contribute to advancing data augmentation methods, which can improve the resilience and applicability of cancer detection algorithms. The capacity to generate a wide range of quality medical images significantly improves the ability to detect diseases early, develop treatment strategies, and improve the overall quality of care for cancer patients.

3.5.5. Vision transformer

The core function of Vision Transformer (ViT) ([Dosovitskiy et al., 2020](#)) is a self-attention mechanism ([Vaswani et al., 2017](#)) that understands the context and accesses previous information. The Vision Transformer (ViT) operates through a sequence of key steps: it first divides the input image into fixed-size patches, each linearly transformed into a vector to form patch embeddings. Positional encodings are added to these embeddings to provide spatial context. The model's core comprises multiple encoder layers, each containing multi-head self-attention (see Equation (8) [Vaswani et al., 2017](#)) and feedforward neural networks. The self-attention mechanism captures relationships between patches, allowing the model to focus on important regions by computing weighted sums of patch embeddings. Following this, feedforward neural networks introduce non-linearity and learn complex relationships. Layer normalization and residual connections stabilize and enhance each sub-layer's outputs, ensuring effective training and preventing vanishing gradients. [Sriwastava and Arul Jothi \(2024\)](#) implemented vision transformer variants for breast cancer detection using Breakhis and IDC datasets. Some vision transformer variants are CvT, CrossFormer,

CrossViT, etc. The related code for each variant can be found on Github.¹

$$\begin{aligned} \text{MultiHead}(M, N, P) &= \text{Concat}(\text{head}_1, \dots, \text{head}_h)W^O \\ \text{where, } \text{head}_i &= \text{Attention}(MW_i^M, NW_i^N, PW_i^P) \\ \text{Attention}(M, N, P) &= \text{softmax}\left(\frac{MN^T}{\sqrt{d_N}}\right)P \end{aligned} \quad (8)$$

3.6. Transfer learning

3.6.1. VGGNet

The VGGNet (Sengupta et al., 2019) architecture is known for its straightforward design, which includes the incorporation of compact 3×3 convolutional filters. The VGG16 and VGG19 are two prominent versions of the VGGNet, which differ in terms of their quantity of trainable parameters and layers. VGG16 is composed of sixteen weight layers, with thirteen being convolutional layers (2 layers of 64 filters, 2 layers of 128 filters, 3 layers of 256 filters, 3 layers of 512 filters, and 3 layers of 512 filters) and three being fully connected (FC) layers (4096, 4096, 1000 units). VGG-19 is more extensive than VGG-16, boasting a total of 16 convolutional layers (2 layers of 64 filters, 2 layers of 128 filters, 4 layers of 256 filters, 4 layers of 512 filters, and 4 layers of 512 filters) and three fully connected (FC) layers (4096, 4096, 1000 units). Both VGG16 and VGG19 have 5 Max-Pooling layers (2×2) after each set of convolutional layers. Although VGGNet is known for its simplicity, it requires a significant amount of processing resources due to its complexity and dependence on 3×3 filters. Because of its simple composition, it has been thoroughly investigated in the field of medical image classification.

3.6.2. ResNet

ResNet (Residual Networks) (Zagoruyko and Komodakis, 2016) is a deep CNN that uses residual learning to enable the training of very deep networks. This is achieved by using skip connections, which effectively address the issue of the vanishing gradient problem. ResNet-50 comprises 50 layers, organized in a sequence of residual blocks, each including three convolutional layers. ResNet-101 enhances this design by including 101 layers using a larger quantity of residual blocks. ResNet-152 is an extension of the ResNet model that increases the depth of the network to 152 layers.

3.6.3. Inception

InceptionNetV1 (Szegedy et al., 2016), or GoogLeNet (Szegedy et al., 2015; Al-Huseiny and Sajit, 2021), is a complex CNN structure that introduced the inception module, a pivotal advancement to enhance computing efficiency while maintaining superior performance. The inception module conducts convolutions using various filter sizes (1×1 , 3×3 , and 5×5) and a 3×3 max pooling operation simultaneously, combining their results along the depth dimension. This enables the network to record many spatial elements and sizes concurrently, enhancing its ability to recognize intricate picture patterns. The first InceptionNet, comprising 22 layers, effectively decreased the parameter count compared to conventional CNNs due to using 1×1 convolutions that reduce dimensionality before performing more computationally intensive procedures. Later iterations, such as InceptionV2, V3, and V4, included improvements and enhancements, such as factorized convolutions and regularization algorithms, resulting in better accuracy and efficiency. The modular and scalable architecture of InceptionNet has had a significant impact, leading to breakthroughs in developing deep learning models for many computer vision applications. The modular and scalable architecture of InceptionNet has significantly impacted the development of deep learning models for a range of computer vision tasks.

3.6.4. DenseNet

DenseNet (Iandola et al., 2014) is a deep learning architecture that aims to enhance the flow of information and gradients within the network. In contrast to CNN, which only has direct connections to its subsequent layers, DenseNet establishes direct connections between each layer and every other layer in a feed-forward manner. This implies that the feature maps from previous layers are utilized as inputs for each layer, and their outputs are transmitted to all subsequent layers. This highly interconnected pattern improves the reuse of features and addresses the issue of the gradient vanishing problem, making it easier to train extremely deep networks. DenseNet architectures, like DenseNet-121, DenseNet-169, and DenseNet-201, are represented by their depth (number of layers) and dense blocks, establishing connections between layers. The connectivity between layers in DenseNets results in better parameter utilization and enhanced performance, making them a powerful tool for image classification and computer vision tasks.

3.6.5. AlexNet

AlexNet transformed image processing by introducing a groundbreaking deep convolutional neural network architecture. AlexNet (Krizhevsky et al., 2017) is composed of a total of eight layers. These layers include five convolutional layers and three fully connected layers. The architecture includes max-pooling layers following specific convolutional layers to decrease spatial dimensions and computational load. AlexNet utilizes ReLU activations to introduce non-linearity, resulting in faster training and addressing the vanishing gradient problem. In addition, dropout is used in the fully connected layers to prevent overfitting. An important breakthrough of AlexNet was the incorporation of data augmentation and GPU acceleration to effectively manage the computational requirements of training on extensive datasets such as ImageNet.

3.6.6. MobileNet

MobileNet is a collection of compact deep neural network structures for efficient implementation in mobile and embedded vision tasks. MobileNet utilizes depthwise separable convolutions to divide the convolution process into two steps: a depthwise convolution and a pointwise convolution. This approach effectively decreases the number of parameters and computing expenses when compared to conventional convolutions. The MobileNet evolution comprises multiple versions: MobileNetV1 (Howard et al., 2017), which proposed depthwise separable convolutions; MobileNetV2 (Sandler et al., 2018), which incorporated inverted residuals and linear bottlenecks to enhance performance and efficiency; and MobileNetV3 (Howard et al., 2019), which integrated advancements such as squeeze-and-excitation modules and neural architecture search (NAS) to improve performance further and decrease latency. MobileNet topologies are very advantageous for cancer detection because they excel at precise image analysis on devices with limited resources. This allows for real-time processing and diagnosis in clinical situations with restricted computing capabilities.

3.7. Evaluation metrics

Evaluation metrics are used to evaluate the model's performance by estimating the accuracy of a model on unseen data samples. Four basic concepts of evaluating metrics are true positive, true negative, false positive, and false negative. These terms are described below:

- True Positive (TP): predicted as true and indeed true.
- True Negative (TN): predicted as false and indeed false.
- False Positive (FP): predicted as true and indeed false.
- False Negative (FN): predicted as false and indeed true.

¹ <https://github.com/lucidrains/vit-pytorch>

3.7.1. Accuracy

Accuracy is the proportion of accurately predicted cases (true positives and true negatives) out of all instances. It quantifies the overall accuracy of the system's predictions.

$$\text{Accuracy} = \frac{TP + TN}{TP + TN + FP + FN} \quad (9)$$

The accuracy of a model that accurately predicts 80 out of 100 malignant photos and detects 90 out of 100 non-cancerous images would be calculated as $(80 + 90) / 200 = 0.85$ or 85 %. This suggests the model accurately predicts outcomes with an 85 % success rate.

3.7.2. Precision

Precision is the quotient obtained by dividing the number of correct positive predictions by the sum of correct positive predictions and incorrect positive predictions. It quantifies the model's precision in correctly detecting positive cases only.

$$\text{Precision} = \frac{TP}{TP + FP} \quad (10)$$

Given a segmentation model that detects 100 areas as malignant, with 80 of them being really cancerous and 20 being false positives, the precision will be calculated as $80 / (80 + 20) = 0.8$ or 80 %. This indicates that the model accurately identifies 80 % of the locations as malignant or diseased.

3.7.3. Recall / sensitivity / true positive rate

Recall, also known as sensitivity, is the proportion of correct positive predictions to the total number of positive predictions, including both true positives and false negatives. The metric quantifies the model's capacity to accurately detect all relevant positive cases.

$$\text{Recall} = \frac{TP}{TP + FN} \quad (11)$$

If there are 100 malignant areas in the dataset and the model accurately detects 80 (missing 20), the recall would be calculated as $80 / (80 + 20) = 0.8$ or 80 %. This suggests the model accurately detects 80 % of the real malignant areas.

3.7.4. F1-score

The F1-score is a statistical measure that calculates the harmonic mean of accuracy and recall, thereby balancing the two measurements. It is advantageous when there is an uneven distribution of classes in the dataset.

$$\text{F1-score} = \frac{2 \cdot \text{Precision} \cdot \text{Recall}}{\text{Precision} + \text{Recall}} \quad (12)$$

Given the precision of 80 % and recall of 80 % from the previous instances, the F1-score can be computed as $2 * (0.8 * 0.8) / (0.8 + 0.8) = 0.80$ or 80 %.

3.7.5. Specificity / true negative rate

Specificity refers to the accuracy of accurately classifying the negative class.

$$\text{specificity} = \frac{TN}{TN + FP} \quad (13)$$

3.7.6. False positive rate and false negative rate

The False Negative Rate (FNR) indicates the percentage of instances belonging to the positive class that were wrongly identified by the algorithm. The false positive rate (FPR) quantifies the proportion of instances from the negative class that the algorithm mistakenly classified as positive. It is preferable to have a greater TNR and a lower FPR to accurately categorize instances of the negative class.

$$\text{FPR} = 1 - \text{specificity} = \frac{FP}{TN + FP} \quad (14)$$

$$\text{FNR} = \frac{FN}{TP + FN} \quad (15)$$

3.7.7. AUC-ROC curve

The AUC-ROC quantifies the model's capacity to differentiate between positive and negative classifications. The ROC curve graphically represents the relationship between the true positive rate (recall) and the false positive rate (1-specificity) at different threshold values.

A cancer detection model with an AUC-ROC value of 0.95 demonstrates exceptional discriminatory power in distinguishing between malignant and non-cancerous areas. This implies that the model has a strong capability to identify both positive and negative cases accurately. A model that is considered flawless has an Area Under the Curve (AUC) value of 1.0, whereas a model that lacks discriminating power has an AUC value of 0.5.

3.7.8. Kappa score

Cohen's Kappa (Cohen, 1960) was first introduced to measure the level of consensus between two analysts who evaluated the same group of individuals using a nominal scale with two or more categories. The metric is often used for binary classification issues.

$$k = \frac{2 \cdot (TP \cdot TN - FP \cdot FN)}{(TP + FP) \cdot (TP + FN) \cdot (TP + FN) \cdot (TN + FN)} \quad (16)$$

3.7.9. Matthews correlation coefficient (MCC)

To address imbalanced datasets, the Matthews correlation coefficient offers an alternative method to calculate the Pearson product-moment correlation coefficient between actual and projected values using a contingency matrix (Chicco and Jurman, 2020). The lowest possible value of MCC is -1, and the highest possible value is +1.

$$\begin{aligned} \text{MCC} &= \frac{(TP \cdot TN) - (FP \cdot FN)}{\sqrt{A \cdot B \cdot C \cdot D}} \\ A &= (TP + FP), B = (TP + FN) \\ C &= (TN + FP), D = (TN + FN) \end{aligned} \quad (17)$$

3.7.10. Jaccard index and dice coefficient

Jaccard Index and Dice Coefficient are the most used evaluation metrics for segmentation. Jaccard index, also known as Intersection-over-Union (IoU) or Jaccard similarity coefficient (see Equation (18)). Dice Coefficient (DC), also known as Sørensen-Dice index (see Equation (19)).

$$\text{Jaccard Index} = \frac{TP}{TP + FP + FN} \quad (18)$$

$$\text{Dice Coefficient} = \frac{2TP}{2TP + FP + FN} \quad (19)$$

4. Case study of cancer detection

This section discusses the case study of cancer, including each cancer dataset and related research works. Figure 3 shows the 12 types of cancers in medical imaging images, including breast cancer (Fig. 3a), cervical cancer (Fig. 3b), ovarian cancer (Fig. 3c), prostate cancer (Fig. 3d), esophageal cancer (Fig. 3e), liver cancer (Fig. 3f), pancreatic cancer (Fig. 3g), colon cancer (Fig. 3h), lung cancer (Fig. 3i), oral cancer (Fig. 3j), skin cancer (Fig. 3k), and brain cancer (Fig. 3l). The Cancer Imaging Archive (TCIA)² include most of the cancer

² <https://wiki.cancerimagingarchive.net/>

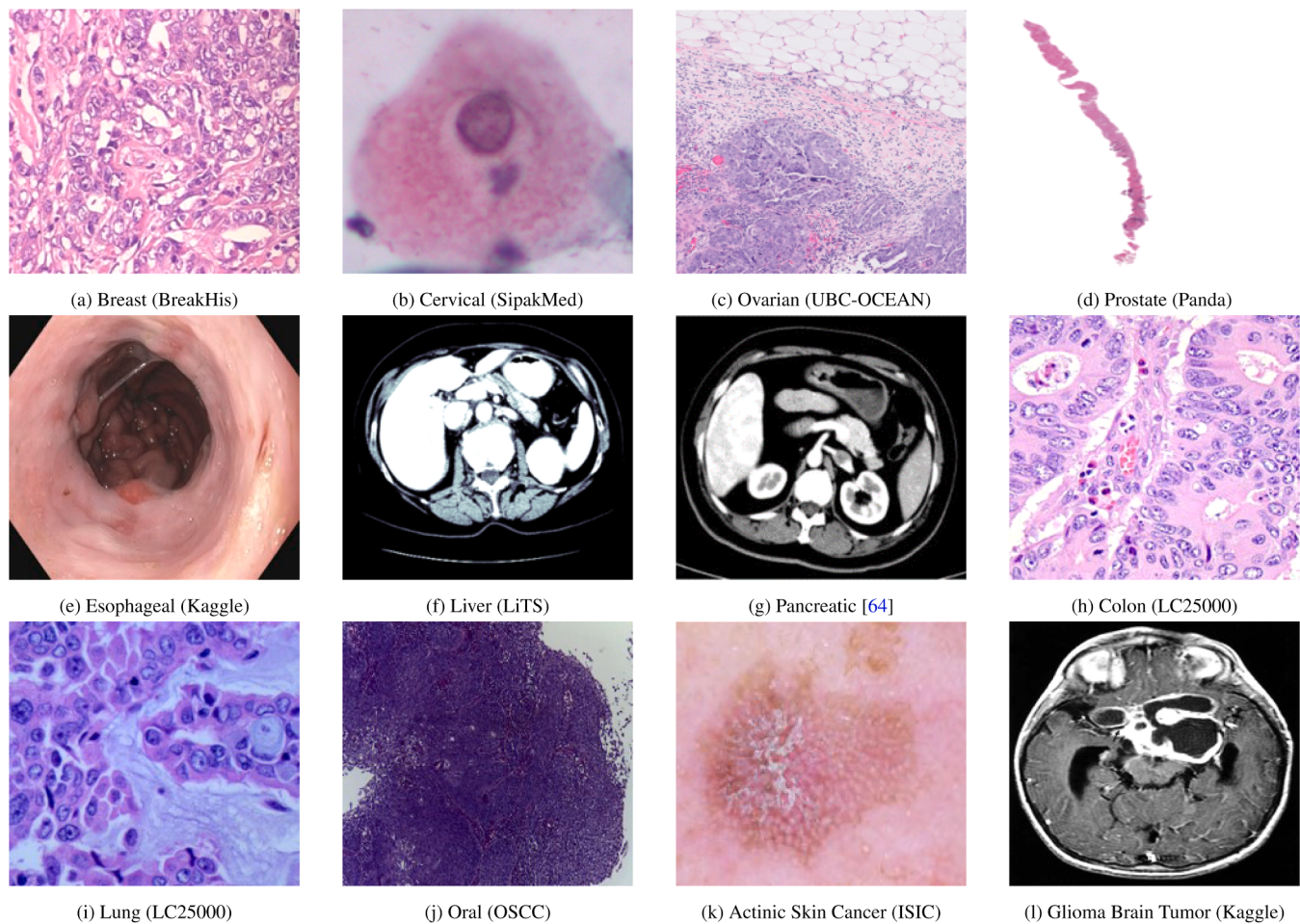


Fig. 3. Different Types of Cancer Image.

dataset for detection and segmentation (Clark et al., 2013). This study used the following acronyms in Tables 4, 5, 6, 7, and 8 to show the existing research outcomes: acc=accuracy, pr=precision, re=recall, and f1=f1-score.

4.1. Reproductive system

4.1.1. Breast cancer

Breast cancer is defined as the uncontrolled growth of breast cells that results in tumour formation. These tumours may spread and potentially lead to death. In 2022, it resulted in a total of 670,000 deaths worldwide. Women account for approximately 50 % of breast cancer occurrences because of their gender and age (Breast cancer, 2024). Men may also be affected by breast cancer; globally, males account for 0.5–1 % of cases (Aygin and Yaman, 2022). Consequently, early detection of this cancer is critical for its treatment. Radiologists diagnose breast cancer using the most accurate procedure known as mammography. Apart from that, other screening tests are breast MRIs and ultrasounds, which diagnose breast cancer.

Breast cancer dataset. Some mammogram image datasets are MIAS (Suckling et al., 2015),³ Mini-MIAS,⁴ INBreast (Moreira et al., 2012),⁵

DDSM (Heath et al., 1998), and CBIS-DDSM (Lee et al., 2017). The Mini-MIAS dataset is a subset of the UK-based Mammographic Image Analysis Society (MIAS) (Suckling et al., 2015) database. It consists of 322 images for 161 cases, each with extensive annotations concerning abnormalities. This dataset is highly helpful for developing and testing fundamental algorithms for breast cancer diagnosis. INBreast is a dataset comprising 410 full-field digital mammograms from 115 cases. It provides high-resolution pictures with precise annotations, making it well-suited for developing sophisticated algorithms and performing tasks that require accurate detection and classification of lesions. Digital Database for Screening Mammography (DDSM) (Heath et al., 1998) contained 55,890 images, including 14 % benign and 86 % malignant. CBIS-DDSM⁶ is an enhanced and carefully selected version of the DDSM. It consists of 2620 studies that have detailed annotations at the pixel level for masses and calcifications. This extensive dataset enables the training of powerful algorithms and the evaluation of their performance, hence promoting the creation of dependable computer-aided diagnosis systems. Li et al. (2021a) employed three datasets, including BreakHis (Spanhol et al., 2015),⁷ BACH (Aresta et al., 2019), and PUIH (Yan et al., 2020). The BreakHis dataset consists of 7909 histopathological images that include three colour channels (RGB) and were captured at four different magnification levels: 40x, 100x, 200x, and 400x. The BACH dataset consists of 400 RGB images, whereas the PUIH dataset has 4020

³ <https://www.repository.cam.ac.uk/items/b6a97f0c-3b9b-40ad-8f18-3d121ef1459>

⁴ <https://www.kaggle.com/datasets/kmader/mias-mammography>

⁵ <https://www.kaggle.com/datasets/ramanathansp20/inbreast-dataset>

⁶ <https://wiki.cancerimagingarchive.net/pages/viewpage.action?pageId=22516629>

⁷ <https://www.kaggle.com/datasets/ambarish/breakhis/data>

Table 4
Reproductive System: Breast Cancer (2020–2024).

Year & Ref.	Dataset	Methodology	Result
2024 Shah et al. (2024)	DDSM	employed DCGAN to generate synthetic mammogram images and validated by radiologists to assess the perceptual quality and realism	t-statistic was 6.35 with a p-value < 0.001
Sriwastava and Arul Jothi (2024)	BreakHis, IDC	used vision transformer variants: ViT, PiT, CvIT, CrossFormer, CrossViT, NesT, MaxViT, and SepViT	acc: 91.57 % (BreakHis), 91.8 % (IDC)
Anas et al. (2024)	INbreast, CBIS-DDSM, BNS	YOLOV5 for mass detection and Mask R-CNN for tumour borders and size detection	FPR: 0.049 %, FNR: 0.029 %, MCC: 92.02 %
Admass et al. (2024)	AFG	proposed locally preserving projection transformation function to ensure local features were retained into the Google inception network	acc: 99.81 %, re: 96.48 %
Khan et al. (2024)	DDSM	employed Decentralized Federated Learning to enable collaborative learning, Ant Colony Optimization for hyperparameter fine-tuning, and Neural Architecture Search for optimizing NN architecture	acc: 93.0 %, re: 92.6 %, specificity: 93.0 % (Benign vs. Malignant)
Wang et al. (2024)	FUSCC, BUSI, BLUI	proposed a two-stage training strategy with D-Net, C-Net, and F-Net: D-Net and C-Net trained on fully annotated images with ROI-and image labels and a self-distillation mechanism squeezes knowledge from the F-net into the D-Net and C-Net to fine-tune them.	acc: 92.46 ± 1.78 , re: 92.86 ± 2.38 , specificity: 92.27 ± 2.17 (BUSI)
Teoh et al. (2024)	mini-MIAS, INBreast, CBIS-DDSM	proposed ensemble optimization (AlexNet, GoogLeNet, VGG16, ResNet-50) to detect and localize areas of microcalcifications	avg. confidence level: 0.9305 and 0.8859 for abnormal and normal cases
Zeng et al. (2024)	BreAKHis	improved ResNet architecture (FastLeakyResNet-CIR)	acc: 98.94 %
2023 Jafari and Karami (2023)	RSNA, DDSM, MIAS	employed pre-trained CNN model for feature extraction and ML algorithms for classification	acc: 92 % (RSNA), 94.5 % (MIAS), 96 % (DDSM)
Sharmin et al. (2023)	IDC	proposed resnet50v2 and ensemble-based ML methods	acc: 95 %, pr: 94.86 %, re: 94.32 %, f1: 94.57 %
Boudouh and Bouakkaz (2023)	Mini-MIAS, DDSM, CMMID	Xception, InceptionV3, ResNet101V2, ResNet50V2, AlexNet, VGG16, VGG19 (InceptionV3)	acc: 99.9 % (ResNet50V2), 99.54 % (InceptionV3)
Strelcenia and Prakoonwit (2023)	WBCD	Kullback-Leibler Divergence Conditional GAN (K-CGAN)	acc: 90.86 %, pr: 97.62 %, re: 77.36 %, f1: 86.31 %

Table 4 (continued)

Year & Ref.	Dataset	Methodology	Result
Fuentes-Fino et al. (2023)	INbreast, CBIS-DDSM, CRC	AlexNet, DenseNet, and MobileNet	acc: 69 % (mobileNet)
Asadi and Memon (2023)	INbreast, BCDR, WBCD	Integrate U-Net for segmentation and ResNet50 for classification	acc: 98.61 %, f1: 98.41 %
Kashyap (2023)	BreakHis, BreCaHad	proposed stochastic dilated residual ghost model for cancer detection	AUC: 96.15
Gade et al. (2023)	infrared image	2D empirical wavelet transform was used for multiscale analysis	99.54 %
Chen et al. (2023)	Private	employed wavelet decomposition and weighted recurrence network	AUC: 0.96
Toma et al. (2023)	BreAKHis	ResNext-50, ResNext-101, DPN131, DenseNet-169 and NASNet-A	acc: 99.8 % (ResNext-50)
2022 Gonçalves et al. (2022)	Infrared image	VGG-16, ResNet-50 and DenseNet-201	f1: 92 % (VGG-16), 90 % (ResNet-50)
Azevedo et al. (2022)	BCDR	proposed quantum neural networks using transfer learning	acc: 84 %
Al Husaini et al. (2022)	DMR	employed inception V3, inception V4, and modified inception MV4	acc: 99.748 %
Dey et al. (2022)	DMR	employed prewitt and roberts for edge detection and DenseNet121	acc: 98.8 %
Lu et al. (2022)	USI	pre-trained ReNet-18 with spatial attention mechanism	acc: 94.10 %, pr: 98.14 %, f1: 96.50 %
Alruwaili and Gouda (2022)	MIAS	ResNet50 and NasNet-mobile network	acc: 89.5 % (ResNet50)
2021 Sánchez-Cauce et al. (2021)	DMR	proposed multi-input model integrating thermal images and clinical data	acc: 97 %, AUCROC: 0.99
Li et al. (2021a)	BreakHis, BACH, PUIH	multi-view attention-guided multiple instance detection network	AUC: 0.99 (BreakHis), 0.98 (BACH), 0.98 (PUIH)
Saber et al. (2021)	MIAS	VGG16, VGG19, ResNet50, InceptionV3, InceptionV2ResNet	acc: 98.96 %, re: 97.83 %, pr: 97.35 %, f1: 97.66 %
2020 Zheng et al. (2020)	TCIA	CNN with AdaBoost	acc: 97.2 %, re: 98.3 %, specificity: 96.5 %
Wang et al. (2020)	private	3D convolutional network	sensitivity: 95 %

RGB images. However, the specific zoom levels for these images have not been disclosed. The BreAKHis dataset has images with a resolution of 700×460 pixels, whereas the BACH and PUIH datasets provide images with a resolution of 2048×1536 pixels.

There are some B-mode breast ultrasound (BUS) imaging databases, such as a private dataset from Fudan University Shanghai Cancer Center (FUSCC) (Wang et al., 2024). The FUSCC dataset contains BUS images that were obtained from an overall 176 individuals, with 89 patients having benign tumours and 87 patients having malignant malignancy. Every patient was assigned a video file, and 10 images were randomly extracted from each ultrasound video. There were a total of 890 benign and 870 malignant samples. The Mindray Resona7 ultrasonic scanner was used to scan all the samples. The scanning was done using the L11-3 linear-array probe. An expert sonologist marked a rectangular region of interest (ROI) on each BUS image to show the extent of the lesion.

Table 5

Reproductive System Cancer (2020–2024).

Year & Ref.	Dataset	Methodology	Result
Cervical	2024 Fahad et al. (2024)	SipakMed, Herlev	employed random forest feature importance and information gain as feature ranking techniques, GCN was introduced for cervical cell types prediction acc: 99.11 % (SipakMed), 98.18 % (Herlev)
	2023 Mazroa et al. (2023)	Herlev	CLAHE was used for contrast enhancement, LeNet model for feature extraction, and Attention-based Long Short-Term Memory with Improved Bald Eagle Search Optimization (IBESO) for classification. acc: 99.26 %, pr: 97.51 %, re: 97.11 %, f1: 97.29 %
	Sahoo et al. (2023)	Sipakmed, Mendeley LBC	proposed fuzzy rank-based ensemble approach by integrating three pre-trained models (VGG, Inception and ResNet) for feature extraction and prediction acc: 97.18 % (Sipakmed), f1: 97.16 % (Sipakmed)
	2022 Ji et al. (2022)	71 film images	proposed unsupervised machine learning method for classification re: 90.9 %, specificity: 100 %
	Devi et al. (2022)	Herlev	proposed segmentation technique based on neutrosophic graph cuts (NGCS) acc: 99.42 %, re: 98.52 %, specificity: 99.42 %
	Elakkia et al. (2022)	MobileODT	proposed faster small-object detection neural networks (fsod-gan) for classification acc: 99 %
	2021 Pirovano et al. (2021)	private dataset	a dataset simulating regions of Pap smears was created for training and testing the classifier. loss function, named classification under regression constraint, was used to train the region classifier acc: 95 %
	Bhatt et al. (2021)	Sipakmed, Herlev	Conv Net with Transfer Learning was used for feature extraction and Gradient-weighted Class Activation Mapping (Grad-CAM) was used for visual localization of lesions in images acc: 99.70 %, pr: 99.70 %, re: 99.72 %, f-beta: 99.63 %, kapp: 99.31 %
Ovarian	2023 Mukhedkar et al. (2023)	Pelvic-CT image	proposed Bi-LSTM with CNN to enhance learning and employed Lion with Grey Wolf Optimization (LGWO) for efficient feature selection acc: 98 %, pr: 93 %, re: 99.7 %, f1: 98 %
	Paayas and Annamalai (2023)	UBC-OCEAN OCT recordings	DenseNet121 employed VGG-supported Feed-forward Network and 3D CNN to capture spatial relationships in data acc: 99.6 %, f1: 100 % AUC: 0.81 ± 0.037
Prostate	2023 Nishio et al. (2023)	Panda	employed EfficientNet B3 and Label distribution learning acc: 40.7 %
	Bashkanov et al. (2023)	1074 mpMRI	3D nnU-Net Architecture was used for anisotropy in MRI data. Cancer findings were categorized into coarse, medium, and fine granularities. Lesion-wise partial FROC-AUC: 1.94
	Wilson et al. (2023)	1028 biopsy cores	Self-Supervised Learning (SSL) is implemented to leverage the abundance of unlabeled micro-ultrasound data AUROC: 91 %
	2021 Duran-Lopez et al. (2021)	Hematoxylin, Eosin-stained slides	CNN is used to obtain patch-level features and aggregated these using custom wide and DNN model acc: 94.24 %, re: 98.87 %
	Qian et al. (2021)	ProstateX, PROMISE12	employed a 3D prostate cancer lesion segmentation network based on focal Tversky loss TPR: 91.82 %
	Iqbal et al. (2021)	Carcinoma Images	Self-Supervised Learning (SSL) is implemented to leverage the abundance of unlabeled micro-ultrasound data acc for GLCM with KNN-cosine: 99.07 % AUC: 0.909 AUROC: 0.882 ± 0.030
	Pinckaers et al. (2021)	4712 biopsy	applied LSTM and ResNet-101 and compared with Hand-Crafted Features (texture, morphology, and GLCM) and ML algorithms deep attention mechanisms were proposed to enhance detection performance, and decoupled residual classifier is used to reduce false positive
	Saha et al. (2021)	1950 bpMRI	proposed ResNet34 for feature extraction Weighted Kappa: 0.13 ± 0.27 (Lesion-wise)
	de Vente et al. (2021)	ProstateX-2	2D U-Net was used to lesion segmentation maps and ensemble approach implemented to enhance the accuracy acc: 99.98 %, f1: 99.98 %, AUC: 0.999
	2020 Duran-Lopez et al. (2020)	private dataset	CNN is employed for cancer detection Weighted Kappa: 0.13 ± 0.27 (Lesion-wise)
	Sedghi et al. (2020)	145 biopsy cores	proposed fully convolutional networks (FCN) based on U-Net and U-Net with attention gates AUC: 0.76

Another private dataset was AFG (Admass et al., 2024), which was developed by Assosa General Hospital, Felege-Hiwot Hospital, and Gondar University Hospital. Some public datasets like BUSI (Al-Dhabyani et al., 2020) and BLUI (Ardakani et al., 2023) are also available for breast cancer detection. The BUSI dataset was gathered from the Baheye Hospital and consisted of data collected in 2018 from 600 female patients aged between 25 and 75 years old. The dataset has 780 images with an average of 500 × 500 pixels. The images are categorized into normal, benign, and malignant. Given that this particular dataset only includes labels and masks at the image level to segment lesions. The BLUI dataset was collected from the Shahid Beheshti University of Medical Sciences. The dataset has a total of 232 BUS images, consisting of 109 benign cases and 123 malignant instances. All images were annotated based on the histopathologic research findings, which included fine needle aspiration, core needle, or open biopsies. The ROI in every image was marked by a radiologist with 20 years of expertise.

Radiological Society of North America (RSNA)⁸ provided 54,713 images in Digital Imaging and Communications in Medicine (DICOM) format from roughly 11,000 patients. The CRC (Calderon-Ramirez et al., 2022) dataset comprises 87 cases of patients aged between 40 and 90

years old, obtained from the private clinic of Chavarria Estrada Medical Imaging in Costa Rica. Silva et al. (2014) proposed an infrared image dataset for breast cancer detection (Gade et al., 2023; Gonçalves et al., 2022). The University of Pennsylvania and the Cancer Institute of New Jersey have presented a histopathological image dataset (Cruz-Roa et al., 2014) comprising 279 whole slide images (WSI) of breast cancer specimens obtained from 162 women. University Hospital Antônio Pedro (HUAP) of the Federal Fluminense University of Brazil provided a Mastology Research (DMR) (Al Husaini et al., 2022; Dey et al., 2022) database for thermal images to detect breast cancer. The invasive Ductal Carcinoma (IDC)⁹ dataset consists of 162 whole slide pictures (WSIs), which were enlarged at 40x. From these images, a total of 277,524 patches were recovered, including 198,738 negative patches and 78,786 positive patches. Admass (Admass et al., 2024) collected breast ultrasound images from Assosa General Hospital, Gondar University Hospital, and Felege-Hiwot Hospital. Wisconsin Breast Cancer Database (WBDC)¹⁰ has 699 records of Fine Needle Aspirates (FNA) generated

⁸ <https://kaggle.com/competitions/rsna-breast-cancer-detection>

⁹ <https://www.kaggle.com/datasets/paultimothymooney/breast-histopathology-images>

¹⁰ <https://archive.ics.uci.edu/dataset/17/breast+cancer+wisconsin+diagnostic>

Table 6
Digestive System Cancer (2020–2024).

	Year & Ref.	Dataset	Methodology	Result
Esophageal	2023 Hosseini et al. (2023)	NA	a systematic review paper of esophageal cancer detection	NA
	2020 Nakano et al. (2020)	endoscopic images	Narrowband Imaging (NBI) and Flexible Spectral Imaging Color Enhancement (FICE) was used to enhance capillary patterns in cancerous areas and Lugol Chromoendoscopy for cancer detection implemented Improved Empirical Wavelet Transform (IEWT) for feature extraction to lower-frequency component, and Deep Learning-based Complex Empirical Wavelet Transform (DL-CEWT) for high-frequency components	acc: 92.17 %, re: 96.6 %, specificity: 91.6 %
	Xue et al. (2020)	endoscopic images	acc: more than 95 %	
Liver	2023 Napte et al. (2023)	LiTS	implemented double-stage Gaussian filtering for image enhancement, Edge Strengthening Parallel UNet (ESP-UNet) to bypass the u-seg and o-seg for liver segmentation and DCNN for classification	acc: 98.60 %
	2022 Othman et al. (2022)	LiTS17, 3D-IRCADb-01	proposed two hybrid model: DeeplapV3 + ResNet-50, and VGG-16 + ResNet-50V2 + U-Net + LSTM	acc: 99.5 %, pr: 86.4 %, re: 97.9 %
	2020 Dong et al. (2020)	custom dataset	proposed Hybridized Fully Convolutional Neural Network for liver tumour detection and segmentation	acc: 99 %
Pancreatic	2023 Naga Ramesh et al. (2023)	CT images	Harris Hawks Optimization (HHO) with debsNet121 was used for feature extraction, and Sparrow Search Algorithm (SSA) was used with CNN-BiLSTM for adjusting hyperparameter	acc: 99.26 %, re: 99.26 %, specificity: 99.26 %
	2021 Li et al. (2021b)	Raman spectroscopic	implemented CNN for pancreatic cancer detection	acc: over 95 %
Colon	2024 Alqahtani et al. (2024)	LC25000	median filtering used for noise removal, Improved Water Strider Algorithm (IWSA)	acc: 99.41 %, pr: 98.52 %, re: 98.51 %, f1: 98.51 %

Table 6 (continued)

Year & Ref.	Dataset	Methodology	Result
		for optimizing hyperparameters of MobileNetV2 to extract the features, and convolutional autoencoder for classification	
2023 Haq et al. (2023)	HT-29	applied ResNet-50 to detect and count of colon cancer	acc: 95.3 %
2022 Sakr et al. (2022)	LC25000	proposed Convolutional Neural Network (CNN) for colon cancer detection	acc: 99.50 %
Talukder et al. (2022)	LC25000	implemented VGG16, VGG19, DenseNet169, DenseNet201 for feature extraction, and RF, SVM, LR, MLP, XGB, and LGB to evaluate the model accuracy	acc: 99.05 % (lung), 100 % (colon), 99.30 % (both)

from breast tissue. Every record has nine properties, consisting of 239 (35.0 %) malignant and 444 (65.0 %) benign samples. Lu et al. (2022) Ultrasound Images Dataset (USI)¹¹ for breast cancer detection.

4.1.2. Cervical cancer

Cervical cancer is the fourth most prevalent disease among women globally, with around 660,000 new cases projected for 2022 (Cervical cancer, 2024). In the same year, 94 % of the 350,000 fatalities caused by cervical cancer took place in low- and middle-income countries. The discrepancy may be attributed to inequitable availability of vaccines, screening, and treatment, along with elevated HIV prevalence and socioeconomic variables, including gender biases and poverty. Women who have HIV have six times greater chance of developing cervical cancer, which accounts for 5 % of all cases.

Cervical cancer dataset. Plissiti et al. proposed a SIPaKMeD (Plissiti et al., 2018) dataset for cervical cancer detection. SIPaKMeD¹² is a publicly available dataset containing 4049 cell images that have been annotated and classified into five categories. There are two categories for normal cells (superficial-intermediate and parabasal cells), two categories for aberrant but non-malignant cells (koilocytes and dyskeratotic cells), and one category for benign (metaplastic) cells. The dataset includes two kinds of images: whole images and cropped cell core data. The cropped data represent a subset of the whole picture extracted from the cell nucleus. The Herlev (Marinakis et al., 2009b; Marinakis et al., 2009a) dataset comprises around 917 cervical cell images obtained at the University Hospital of Herlev using a digital camera and microscope. The Herlev dataset consists of seven distinct types of cervical cells: superficial squamous, severe dysplasia, columnar epithelium, moderate dysplasia, carcinoma, mild dysplasia, and intermediate squamous, with 150, 146, 192, and 182 images corresponding to cancer, moderate dysplasia, severe dysplasia, and mild dysplasia, respectively. MobileODT¹³ is a Kaggle competition dataset for cervical cancer screening.

¹¹ <https://www.kaggle.com/datasets/aryashah2k/breast-ultrasound-images-dataset>

¹² <https://www.kaggle.com/datasets/prahladmehendiratta/cervical-cancer-largest-dataset-sipakmed>

¹³ <https://www.kaggle.com/c/intel-mobileodt-cervical-cancer-screening/overview>

Table 7
Respiratory System Cancer (2020–2024).

	Year & Ref.	Dataset	Methodology	Result
Lung	2024 Nair and Jerome (2024)	Private dataset	Combined PET and MRI images at the pixel level, applied Adaptive Tee Seed Optimization for selecting optimal fusion parameters and Deep Extreme Learning Machine as a classifier	acc: 97.23 %
Noaman et al. (2024)	LC25000, BreakHis		DenseNet201 for feature extraction, and KNN, SVM, LGBM, catboost, XGBoost, DT, RF, MultinomialNB for classification.	acc: 99.68 % (LC), acc: 94.808 % (Br.)
2023 Malik et al. (2023)	LC chest X-ray		Proposed CDC Net (a CNN incorporating residual network concepts and dilated convolution) for COVID-19, lung cancer, pneumothorax, tuberculosis, and pneumonia classification	acc: 99.39 %, re: 98.13 %, pr: 99.42 %, AUC: 0.9953
Obayya et al. (2023)	Biomedical images		Gabor Filtering applied image preprocessing, GhostNet for feature extraction, Adaptive Fuzzy Artificial Optimizer to adjust GhostNet hyperparameters, and Tuna Swarm Algorithm combined with Echo State Network for lung and colon cancer detection	acc: 99.33 %
Chikkalingaiah et al. (2023)	LIDC		median filter for noise removal, GLCM for feature extraction, and SVM, RF, KNN, and DT are used for classification	acc: 99.32 % (SVM)
2022 Jain et al. (2022)	LC25000, NLST, NCI		Kernel Principal Component Analysis integrated with CNN for feature extraction, and Fast Deep Belief Neural Network for classification	acc: 97.1 % (LZ2500), 98 % (NLST), 97.5 % (NCI)
Liberini et al. (2022)	regenerate PET/CT		highest detectability for BSREM200 and BSREM300	
Bhattacharjee et al. (2022)	LIDC-IDRI		Maximization with different β -values and Ordered Subset Expectation Maximization optimized random forest with K-means visualization	acc: 92.14 %

Table 7 (continued)

	Year & Ref.	Dataset	Methodology	Result
	2021 Alzubaidi et al. (2021)	1000 CT	ten different feature types are used, including Gabor filter, Histogram of Oriented Gradients (HOG), andhaar wavelet and six ML algorithms	acc: 97 %, re: 96 %, and specificity: 97 %
	Lu et al. (2021)	RIDER	MPA optimization algorithm with CNN to enhance the accuracy and compared with ResNet-18, GoogLeNet, AlexNet, and VGG-19	acc: 93.4 %, re: 98.4 %, specificity: 97.1 %
	2020 Rajagopalan and Babu (2020)	JSRT	Implemented a Massive ANN-based soft tissue technique and Recognizes nodule candidates from X-ray images for feature extraction and classification	acc: 72.96 % (with soft tissue), 66.76 % (without)
	Chenyang and Chan (2020)	LUNA16, LIDC-IDRI	proposed 3-d encoder-decoder architecture for automatic cancer and nodules detection	acc: 90.29 %, re: 88.79 %, specificity: 91.78 %
	Masood et al. (2020b)	LIDC	Multidimensional Region-based Fully Convolutional Network (MRFCN) for detection and classification	acc: 97.91 %, re: 98.1 %
	Masood et al. (2020a)	LUNA16, ANODE09, LIDC-IDRI	proposed 3d deep convolutional neural network and applied median intensity projection and multi-region proposal network (mrpn) for automatic selection of potential 3D region-of-interests	acc: 98.51 %, re: 98.4 %, specificity: 92 %, auroc: 92 %
	Oral 2024 Deo et al. (2024)	H&E dataset	ensemble of DL models (ResNet50 and DenseNet201)	acc: 92 %
	2023 Myriam et al. (2023)	LT dataset	CNN and DBN with particle swarm and al-biruni earth radius optimization	acc: 97.35 %
	2022 Marzouk et al. (2022)	LT dataset	Fuzzy-based contrast enhancement, DenseNet-169 for feature extraction and COA optimization algorithms + Autoencoder for classification	acc: 90.08 %
	Shamim et al. (2022)	private dataset	pre-trained models, including AlexNet, GoogLeNet, Vgg19, ResNet50, Inceptionv3 and SqueezeNet are used to detect binary and five types of tongue lesions	binary acc: 97.5 % (vgg19), multi-class acc: 96.7 % (resnet50)

(continued on next page)

Table 7 (continued)

Year & Ref.	Dataset	Methodology	Result
2021 Yan et al. (2021)	62 healthy–62 patients	variations of Emission Filters and 264 classifiers formed from the combination of four quantization methods, two excitation sources, and 30 spectral bands	acc: 82.85 %, recall: 96.15 %
2020 Welikala et al. (2020)	MEMOSA	ResNet101 for image classification and Faster R-CNN for object detection	f1: 87.07 % & 41.18 % for classification & detection

Table 8
Other System (2020–2024).

Year & Ref.	Dataset	Methodology	Result
Skin	2024 Midasala et al. (2024)	ISIC 2020	Bilateral filter to remove noise; multilevel (low-level, texture, and colour) feature extraction using GLCM, RDWT and K-means clustering (KMC) for segmenting.
	Naeem et al. (2024)	ISIC 2019	DL models and Handcrafted methods for feature extraction, and CNN for classification
	Alqarafi et al. (2024)	Med-node, ISIC, DermIs	MEWF for noise reduction, M-GCN for feature extraction, Tri-level feature fusion module and sigmoid function for classification
	2023 Kavitha et al. (2023)	ISIC 2018	MEWF for noise reduction, M-GCN for feature extraction, Tri-level feature fusion module and sigmoid function for classification
	2022 Fraiwan and Faouri (2022)	HAM10000	auto correlogram methods, color layout filter, binary pyramid pattern filter, ensemble models used for detection
	Mohakud and Dash (2022)	ISIC	ensemble models used for detection
	Imran et al. (2022)	ISIC	thirteen transfer learning model used for classification
	2021 Wang and Hamian (2021)	SIIM-ISIC	GWO algorithm used to optimize CNN hyper-parameters and compared with PSO and GA
	Huaping et al. (2021)	ACS, PH2	ensemble learning technique using VGG, capsnet, resnet
	2020 Wei et al. (2020)	ISIC 2016	acc: 99.18 %, fpr: 99.25 %, pf: 99.04 %, MCC: 99.84 %
Brain	Ashraf et al. (2020)	DermIs and DermQuest	acc: 97.81 %, pr: 98.31 %, re: 97.89 %, f1: 98.10 %
	Thanh et al. (2020)	ISIC	acc: 98.78 %, re: 97.99, f1: 98.84 %
	2024 Kumar et al. (2024)	MRI scans (private)	acc: 90.96 %, pr: 91 %, re: 91 %, f1: 0.91 %
	2023 Mercaldo et al. (2023)	Br35H	acc: 82.9 %
	2020 Florimbi et al. (2020)	HSI data	acc: 98.33 %
			acc: 93.5 %, re: 87 %, specificity: 94 %
			acc: 92.65 %, re: 91.18 %, specificity: 89.70 %
			acc: 64.19 %, 70 % (PH2)
			acc: 96.2 %, ji: 86.7 %, dc: 92.3 %
			acc(dermis): 97.9 %, acc(dermquest): 97.4 %
			acc: 96.6 %, dice: 93.9 %, jaccard: 88.7 %
			acc: 97 %
			acc: (97.83 % - 99.67 %)
			classify large image dataset under 3 s

The dataset has three cervix types, including type 1 (completely ectocervical and fully visible), type 2 (has endocervical component and fully visible), and type 3 (has endocervical component and not fully visible). Mendeley Liquid-based cytology (LBC) (Hussain, 2019) comprises pap smear images from 460 patients captured in 40x magnification.

4.1.3. Ovarian cancer

Ovarian cancer (Ovarian, fallopian tube, and primary peritoneal cancer, 2024) is a malignant tumor that originates in the ovaries, which are an integral element of the female reproductive system. It mostly affects aging women between 50 and 70. It is more frequent in persons with a family history of ovarian or breast cancer, genetic abnormalities such as BRCA1 or BRCA2, or who have never been pregnant. Common symptoms of ovarian cancer often include chronic bloating, abdominal pain, impaired appetite or early satiety, and frequent or urgent urine. These symptoms are often inconspicuous and might be misinterpreted as less severe illnesses, resulting in a delayed diagnosis. Timely identification is essential since ovarian cancer is often detected in a late stage, when it has already metastasized, making treatment more challenging.

Timely detection greatly enhances the chances of survival and treatment results, underscoring the need for routine screens and knowledge of symptoms.

Ovarian cancer dataset. UBC-OCEAN (Paayas and Annamalai, 2023)¹⁴ comprises five distinct subtypes of ovarian cancer: high-grade serous carcinoma, low-grade serous, endometrioid, clear-cell ovarian carcinoma, and mucinous carcinoma. There are two distinct classifications of images: whole slide images (WSI) and tissue microarray (TMA). The WSI is magnified by a factor of 20 and might be of considerable size. The TMAs have a lower size, around 4,000x4000 pixels, but they are magnified at a factor of 40x.

4.1.4. Prostate cancer

The prostate is a male reproductive system that comprises three

distinct regions: the transition zone, central zone, and peripheral zone, with the latter two forming around 95 % of its total volume. The majority of prostate cancer cases, about 70 %, are discovered in the peripheral zone, while just 2.5 % of cases happen within the transition zone. Although the transition zone is the smallest area, it has a 20 % likelihood of getting prostate cancer (McNeal et al., 1988). Timely detection greatly enhances the chances of survival and treatment results, underscoring the need for routine screens and knowledge of symptoms.

Prostate cancer dataset. ProstateX (Litjens et al., 2014a) is a collaborative medical image detection competition sponsored by the American Association of Physicists in Medicine (AAPM), the International Society for Optics and Photonics (SPIE), and the National Cancer Institute (NCI). The ProstateX collection comprises MR images with several sequences, including T2-weighted (T2 W) images, proton density-weighted (PD-W) images, dynamic enhancement (DCE) images, and diffusion-weighted

¹⁴ <https://www.kaggle.com/competitions/UBC-OCEAN>

(DW) images. The label file given by ProstateX contains the precise coordinates of the lesion and information on whether it is benign or cancerous. In ProstateX, two sets of patients are included: 204 with 330 lesions in the training set and 142 with 208 lesions in the testing set. The ProstateX-2 (Abraham and Nair, 2018) challenge train set has 99 patients and 112 lesions, and the test set has 63 patients and 70 lesions. The International Medical Image Processing Committee conducted the PROMISE12 (Litjens et al., 2014b) challenge in 2012, focusing on prostate segmentation. The dataset comprises 50 training samples with a T2-weighted sequence of the prostate MR image and its related prostate mask, as well as 30 testing samples. Panda (Prostate Cancer Grade Assessment) (Bulten et al., 2022; Tolkach et al., 2023)¹⁵ challenge comprises a total of 10,616 WSIs, which were obtained from Radboud University Medical Center and Karolinska Institute, totalling 5160 and 5456 WSIs images, respectively. Duran-Lopez et al. (2021) used Hematoxylin and Eosin (H&E)-stained slides (158 normal WSIs and 174 malignant WSIs) for prostate cancer detection.

4.1.5. Summary of reproductive system cancer

Table 4 summarises the list of research articles related to breast cancer, and Table 5 lists the summary of other reproductive system cancer detection studies.

4.2. Digestive system

4.2.1. Esophageal cancer

Esophageal cancer is a malignant tumour originating in the esophagus, the anatomical structure connecting the neck to the stomach. Primarily afflicting the elderly, especially males, this condition is often linked to risk factors such as smoking, excessive alcohol intake, and persistent acid reflux. Common symptoms include dysphagia, angina, unintended weight loss, and a persistent cough. It is categorized into esophageal adenocarcinoma and esophageal squamous cell carcinoma (Esophageal cancer, 2024). It is projected that in the coming years, the rate of this disease, which is now the seventh most frequent cancer worldwide and the sixth largest cause of cancer-related mortality, will rise by 140 % (Stabellini et al., 2022).

Esophageal cancer dataset. Xue et al. (2020) presented a robust method for detecting esophageal cancer using an improved empirical wavelet transform (IEWT) on images obtained from endoscopic procedures. The process involved converting endoscopic images into the L*x*y* colour space and creating a fusion image using the x* and y* components. This fusion image was then analyzed using a mix of wavelet transforms, including a lower-frequency element from IEWT and high-frequency elements from a Deep Learning-based Complex Empirical Wavelet Transformation (DL-CEWT). The technique rigorously determined fractal sizes through box interpolation to identify abnormal areas based on their fractal dimensions. This proposed method significantly enhanced the precision and effectiveness of cancer detection compared to established methods such as SVM, RF, and CNN. Nakano et al. (2020) introduced a minimally intrusive method for differentiating between benign and malignant tissues using low-concentration Lugol staining and narrowband light. The suggested endoscopic system, which collects RGB images synced with narrowband light, had encouraging outcomes in studies conducted with resected material. While more validation and system modifications remain necessary, this technique could potentially improve the precision and sensitivity of esophageal cancer detection in clinical settings.

4.2.2. Liver cancer

Liver cancer is a malignancy originating in the liver cells and

typically impacts people with chronic liver illnesses like hepatitis or cirrhosis. It can happen in adults and children. Common symptoms of this condition include decreased appetite, discomfort in the upper abdomen, feelings of nausea, and the manifestation of jaundice (Liver and bile duct cancer, 2024). Timely identification is important for liver cancer as it significantly improves the efficacy of therapy, elevates survival rates, and permits less intrusive procedures. The estimated number of new cases of liver cancer and deaths in 2024 are 41,630 and 29,840, respectively (Cancer stat facts: Liver and intrahepatic bile duct cancer, 2024).

Liver cancer dataset. The LiTS (Bilic et al., 2023; Chlebus et al., 2018) challenge comprises 131 contrast-enhanced abdomen CT images obtained from 7 different clinical institutes. Expert radiologists have conducted liver and tumour reference annotations to accompany the CT images. The horizontal resolution varies between 0.5 and 1.0 mm, while the vertical thickness spans from 0.7 to 5.0 mm. The dataset comprises 908 lesions, with 63 % having the longest axial diameter of 10 mm or more. The 3D-IRCADb01 (Soler et al., 2010) dataset comprises 20 3D CT images obtained from 20 distinct patients, with liver tumours present in 75 % of the cases. Each image has dimensions of 512 × 512 pixels and exhibits varying average liver densities ranging from 40 to 135. The images with labels were partitioned into segments using the DICOM format.

4.2.3. Pancreatic cancer

Pancreatic cancer is a malignant tumour originating in the pancreas tissues. According to the National Cancer Institute (Cancer stat facts: Pancreatic cancer, 2024), the estimated number of new cases of pancreatic cancer and deaths in 2024 are 66,440 and 51,750, respectively.

Pancreatic cancer dataset. Naga Ramesh et al. (2023) employed Harris Hawks Optimization (HHO) with debsNet121 for feature extraction and Sparrow Search Algorithm (SSA) with CNN-BiLSTM for adjusting hyperparameters. They used a CT image dataset containing 250 pancreatic tumours and 250 non-pancreatic tumour images. Li et al. (2021b) used CNNs to improve the recognition of pancreatic cancer via the use of spontaneous Raman spectroscopy. The work entailed the examination of 1D and 2D Raman images of pancreatic tissue in a mouse model to assess the efficacy of CNNs in detecting malignant areas. The authors emphasized the significance of visualizing crucial features from the CNN models, as it facilitates the precise identification of malignancy. The findings indicate that using CNN-assisted Raman spectroscopy may greatly enhance the detection of pancreatic cancer, implying a hopeful method for early diagnosis and improved treatment results.

4.2.4. Colon cancer

Colorectal cancer is a common and deadly disease, especially in people over 50. The most common symptoms are constipation, abdominal pain, diarrhea, and sudden weight loss. Early detection, through screenings and a healthy lifestyle, can significantly reduce the risk and improve outcomes. By 2040 (Colon cancer, 2023), projections indicate a sharp rise in the global burden of colorectal cancer, with 3.2 million new cases and 1.6 million deaths annually, underscoring the need for effective detection and prevention strategies.

Colon cancer dataset. The histopathological images, LC25000¹⁶ (Alqahtani et al., 2024; Sakr et al., 2022; Talukder et al., 2022), comprise two distinct datasets, one for lung cancer and one for colon cancer. The dataset includes 25,000 images, of which 10,000 are related

¹⁵ <https://www.kaggle.com/competitions/prostate-cancer-grade-assessment>

¹⁶ <https://www.kaggle.com/datasets/andrewmvd/lung-and-colon-cancer-histopathological-images>

to colon cancer and 15,000 to lung cancer. The lung cancer dataset has three distinct categories of cells: adenocarcinomas, squamous cell carcinomas, and benign tissue. The colon cancer dataset has two distinct categories of cells: adenocarcinomas and benign tissue. The LC25000 dataset was created using a portion of HIPAA-compliant information and validated references, incorporating 750 lung tissue samples (250 adenocarcinomas, 250 squamous cell carcinomas, and 250 benign tissue) and 500 colon tissue samples (250 adenocarcinomas and 250 benign tissue). These samples were then augmented to produce a total of 25,000 images.

Haq et al. (2023) introduced the HT-29 cells dataset to detect, classify, and quantify colon cancer cells via image processing and deep learning methods. The HT-29 cell lines were obtained from Procell Life Science and Technology Co. Ltd. The dataset consisted of 566 images classified into two categories: benign and malignant. The ResNet50 model was used for classification, resulting in a validation accuracy of 95.3 %.

4.2.5. Summary of digestive system cancer

Table 6 lists the summary of digestive system cancer detection studies.

4.3. Respiratory system

4.3.1. Lung cancer

Lung cancer is an uncontrolled cell growth in the lungs that causes significant death and disability. The major types of carcinoma are non-small cell carcinoma (NSCLC), defined as a moderate growth rate, and small cell carcinoma (SCLC), defined as a rapid growth rate. Lung cancer continues to be the primary cause of cancer-related mortality worldwide, resulting in about 1.8 million deaths in 2020 (GLOBOCAN 2020). The basic symptoms of this cancer include a persistent cough, chest pain, and breathing difficulty (Lung cancer, 2023).

Lung cancer dataset. The LC25000 (Noaman et al., 2024) dataset comprises 25,000 histological images for lung and colon cancer detection. Malik et al. (2023) used an LC dataset (Shiraishi et al., 2000) that includes around 20,000 chest X-rays and CT scan images. However, they only used LC chest X-ray images with pneumothorax, COVID-19, and tuberculosis images for multi-classification. Alzubaidi et al. (2021) used 1000 CT images collected from the TCIA (Clark et al., 2013) database, including 500 normal and 500 abnormal cases.

The Lung Image Database Consortium and Image Database Resource Initiative (LIDC-IDRI) (Armato et al., 2011) is the most used helical CT images database for lung cancer detection (Bhattacharjee et al., 2022; Chenyang and Chan, 2020; Masood et al., 2020a; Masood et al., 2020b; Chikkalingaiah et al., 2023). This database, stored in DICOM format, has a total of 125 GB and includes 1018 CT scans and 7371 nodules, with annotations by four radiologists available in Extensible Markup Language (XML) files. Nodules fall into three categories: (a) nodules that measure between 3 mm and 30 mm are called nodules; (b) nodules smaller than 3 mm are called non-benign nodules; and (c) non-nodules that are 3 mm or larger and do not exhibit nodule characteristics.

Reference Image Database to Evaluate Therapy Response (RIDER¹⁷) (Lu et al., 2021) dataset developed by the Cancer Research and Prevention Foundation (CRPF) and NCI's centre with the support of RSNA in 2004. This dataset comprises CT images obtained from several lung CT scans ("coffee break experiment") of 32 participants diagnosed with lung cancer. Furthermore, it also includes a database of identified lesions, each of which underwent 2 CT tests using the same machine and imaging technique.

Japanese Society of Radiological Technology (JSRT¹⁸) (Rajagopalan

and Babu, 2020) contains 233 images including 93 normal and 142 nodule x-ray images. LUNA16 (Setio et al., 2017; Chenyang and Chan, 2020; Masood et al., 2020a) is a subset of the LIDC-IDRI dataset. ANODE09 (Van Ginneken et al., 2010; Masood et al., 2020a) comprises 55 CT scans, including five annotations accomplished by three professionals comprising 31 normal and 39 nodules. (Jain et al., 2022) employed three datasets, including LC2500, NLST, and NCI, for lung cancer detection. The NLST (National Lung Screening Trial) dataset includes 215 tiles of size 512 × 512 chosen from original high-resolution histopathological images, with an experienced pathologist manually annotating 83,245 nuclei objects. The NCI Genomic dataset comprises freely available lung cancer images utilised to study the automatic classification of immediate tumours and solid tissue normal using 459 and 1175 eosin-stained histopathology images. Additionally, a set of 567 and 608 WSI is utilized to classify primary tumours.

4.3.2. Oral cancer

The incidence rates of oral cancer have slightly increased for both genders between the mid-2000s and 2015–2019. The age-adjusted occurrence rate for Black males decreased from 31.5 per 100,000 in 1987–12.8, while for Black women it decreased from 12.8 to 4.9. In contrast, the frequency of occurrences among individuals of White ethnicity increased from 10.6 in 2004–18.4 in the period of 2015–2019 (Oral cancer incidence (new cases) by age, race, and gender, 2024).

Oral cancer dataset. Rahman et al. (2020) proposed an archive that encompasses a collection of 1224 histological images detailing the oral cavity, organized into two distinct categories based on resolution. The initial category comprises 89 images depicting normal epithelium alongside 439 images of Oral Squamous Cell Carcinoma (OSCC), each magnified at 100x. Meanwhile, the subsequent category includes 201 images of normal epithelium and 495 images of OSCC, with these specimens magnified at 400x. These images were captured utilizing a Leica ICC50 HD microscope and applied to H&E stained tissue slides (Deo et al., 2024), which were prepared by healthcare experts from a sample pool of 230 patients. Myriam et al. (2023) used Kaggle Lips and Tongue (LT)¹⁹ dataset, comprises 87 malignant images and 44 benign images, resulting in a total of 131 images. They got 97.35 % accuracy for cancer detection. Marzouk et al. (2022) also used the LT dataset and achieved 90.35 % accuracy.

Cancer Research Malaysia originated a mobile application named Mobile Mouth Screening Anywhere (MEMOSA) (Haron et al., 2020) to develop annotated oral session images. Welikala et al. (2020) collected 2155 oral cavity images from 1085 people with and without lesions. The highest and lowest pixels were 5472x3648, and 119x142 pixels, respectively. They used MEMOSA to annotate these collected images.

4.3.3. Summary of Respiratory System Cancer

Table 7 lists the summary of Respiratory system cancer detection studies.

4.4. Other system

4.4.1. Brain cancer

According to the National Cancer Institute (Cancer stat facts: Brain and other nervous system cancer, 2024), the estimated number of new cases of brain and other nervous system cancer is 25,400, and the estimated number of deaths is 18,760 in 2024. The five years (2014–2020) relative survival rate of brain cancer is 33.4 %. Approximately 1 million Americans have a primary brain tumour, with 94,390 new cases expected in 2023, with 59 % occurring in females and 41 % in males (Brain tumor facts, 2024).

¹⁷ <https://wiki.cancerimagingarchive.net/display/Public/RIDER+Lung+CT>

¹⁸ <http://db.jsrt.or.jp/eng.php>

¹⁹ <https://www.kaggle.com/code/shivam17299/oral-cancer-lips-and-tongue-images-dataset/data>

Brain cancer dataset. Br35H²⁰ (Mercaldo et al., 2023) contains a total of 3000 images including 1500 tumorous MRI images and 1500 non-tumorous images. Other studies employed private datasets (MRI scans Kumar et al., 2024, and HSI Florimbi et al., 2020) for brain tumour detection.

4.4.2. Skin cancer

According to the National Cancer Institute (Cancer stat facts: Melanoma of the skin, 2024), the estimated number of new cases of skin cancer is 100,640, and the estimated number of deaths is 8290 in 2024. The five-year (2014–2020) relative survival rate of skin cancer is 94.1 %.

Skin cancer dataset. The International Skin Imaging Collaboration (ISIC)²¹ (Mohakud and Dash, 2022; Imran et al., 2022; Thanh et al., 2020) challenges have emerged as a catalyst for study in the domain of melanoma categorization (Cassidy et al., 2022). The provider offers digitized, high-quality skin lesion images with professional annotations and metadata. From 2016–2020, the ISIC datasets progressively expanded, with ISIC 2016 (Gutman et al., 2016; Wei et al., 2020) containing 1279 images (900 train, 379 test, with two classes: benign and malignant), ISIC 2017 (Codella et al., 2018) having 2600 images (2000 train, 600 test, with three classes: melanoma, seborrheic keratosis, and others), ISIC 2018 (Codella et al., 2019; Kavitha et al., 2023) including 11,527 images (10,015 train, 1512 test, with seven classes: melanoma, melanocytic nevus, basal cell carcinoma, actinic keratosis, benign keratosis, dermatofibroma, vascular lesion), ISIC 2019 (Combalia et al., 2019; Naeem et al., 2024) comprising 33,569 images (25,331 train, 8238 test, with eight classes: ISIC 2018 classes and squamous cell carcinoma), and ISIC 2020 (Rotemberg et al., 2021; Midasala et al., 2024) encompassing 44,108 images (33,126 train, 10,982 test, with nine classes). Additionally, SIIM-ISIC²² is another version of ISIC datasets.

HAM10000²³ (Fraiwan and Faouri, 2022) comprises 11,526 images including 10,015 training images, and 1511 test images from ISIC dataset. Dermis and DermQuest²⁴ (Alqarafi et al., 2024; Ashraf et al., 2020) comprises 206 dermoscopic images. American Cancer Society (ACS)²⁵ (Skin cancer, 2024; Huaping et al., 2021) database comprises 68 pairs of XLM and TLM images. The PH2²⁶ (Mendonça et al., 2013; Huaping et al., 2021) contains 200 dermoscopic images (40 melanomas, 80 nevi, and 80 atypical nevi). MED-NODE²⁷ comprises 170 images (100 nevi and 70 melanoma cases).

4.4.3. Summary of other system cancer

Table 8 lists the summary of brain tumour and skin cancer detection studies.

5. Research summary and discussion

This section discusses the research summary and responds to the stated research questions (RQ). The responses to the research questions are as follows:

RQ 1. a: The challenges associated with medical data are imbalanced datasets, labelling errors, and limited data availability 5.1.1.

RQ 1. b: The preprocessing techniques include several filtering approaches (Gaussian filter, median filter, bilateral filter, etc.), augmentation, noise removal, etc. The details are discussed in Section 3.2.

RQ1. c: The benchmark datasets for cancer detection are discussed in Section 4. The breast cancer detection dataset includes DDSM (Shah et al., 2024; Khan et al., 2024; Jafari and Karami, 2023; Boudouh and Bouakkaz, 2023) CBIS-DDSM (Teoh et al., 2024; Fuentes-Fino et al., 2023), INBreast (Anas et al., 2024; Teoh et al., 2024; Fuentes-Fino et al., 2023; Asadi and Memon, 2023), MIAS (Jafari and Karami, 2023; Alruwaili and Gouda, 2022; Saber et al., 2021), mini-MIAS (Teoh et al., 2024; Boudouh and Bouakkaz, 2023), IDC (Sharmin et al., 2023), BreaKHis (Zeng et al., 2024; Kashyap, 2023; Toma et al., 2023; Li et al., 2021a), CMMD (Boudouh and Bouakkaz, 2023), WBCD (Strelcenia and Prakoonwit, 2023; Asadi and Memon, 2023), BCDR (Asadi and Memon, 2023; Azevedo et al., 2022), and DMR (Al Husaini et al., 2022; Dey et al., 2022; Sánchez-Cauce et al., 2021). Cervical cancer detection datasets are SipakMed (Fahad et al., 2024; Sahoo et al., 2023; Bhatt et al., 2021), and Herlev (Fahad et al., 2024; Mazroa et al., 2023; Devi et al., 2022; Bhatt et al., 2021). Ovarian cancer detection datasets are UBC-OCEAN (Paayas and Annamalai, 2023) and Pelvic-CT (Mukhedkar et al., 2023). Prostate cancer detection datasets are panda (Nishio et al., 2023), ProstateX (Qian et al., 2021), ProstateX-2 (de Vente et al., 2021), and PROMISE12 (Qian et al., 2021). The liver cancer detection datasets are LiTS (Napte et al., 2023; Othman et al., 2022) and 3D-IRCADb-01 (Othman et al., 2022). The Colon cancer detection datasets are LC25000 (Sakr et al., 2022; Talukder et al., 2022) and HT-29 (Haq et al., 2023). Lung cancer detection datasets are LC25000 (Noaman et al., 2024; Jain et al., 2022), LIDC-IDRI (Chikkalingaiah et al., 2023; Bhattacharjee et al., 2022; Chenyang and Chan, 2020; Masood et al., 2020b; Masood et al., 2020a), LUNA16 (Chenyang and Chan, 2020; Masood et al., 2020a), JSRT (Rajagopalan and Babu, 2020), and RIDER (Lu et al., 2021). The oral cancer detection datasets are the LT dataset (Myriam et al., 2023; Marzouk et al., 2022), the H&E dataset (Deo et al., 2024), and MEMOSA (Welikala et al., 2020). The skin cancer datasets are IISC (Midasala et al., 2024; Naeem et al., 2024; Alqarafi et al., 2024; Kavitha et al., 2023; Mohakud and Dash, 2022; Imran et al., 2022; Wei et al., 2020; Thanh et al., 2020), HAM10000 (Fraiwan and Faouri, 2022), ACS, PH2, DermIS and DermQuest (Alqarafi et al., 2024; Ashraf et al., 2020), and Med-Node (Alqarafi et al., 2024). Brain cancer detection datasets are Br35H (Mercaldo et al., 2023) and HSI (Florimbi et al., 2020).

RQ 2. a: The most used deep learning algorithms are CNN (Wang et al., 2024; Mukhedkar et al., 2023; Schwartz et al., 2022; Duran-Lopez et al., 2021; Duran-Lopez et al., 2020; Naga Ramesh et al., 2023; Sakr et al., 2022; Malik et al., 2023; Myriam et al., 2023; Mohakud and Dash, 2022), LSTM (Mazroa et al., 2023), BiLSTM (Mukhedkar et al., 2023; Naga Ramesh et al., 2023; Jain et al., 2022), RCNN (Welikala et al., 2020), GAN (Shah et al., 2024; Strelcenia and Prakoonwit, 2023; Elakkiya et al., 2022), and vision transformer (Sriwastava and Arul Jothi, 2024). The details are discussed in Section 3.5.

RQ 2. b: The most used feature extraction algorithms are GLCM (Midasala et al., 2024), HOG (Alzubaidi et al., 2021), RDWT (Midasala et al., 2024) and wavelet transform (Xue et al., 2020; Alzubaidi et al., 2021). The details are discussed in Section 3.4.

RQ 2. c: Leveraging pre-trained models through transfer learning can substantially bolster the performance of deep learning models in detecting cancer, particularly when working with limited datasets, leading to more accurate and reliable results. The most used pre-trained models are VGG16 (Teoh et al., 2024; Boudouh and Bouakkaz, 2023; Gonçalves et al., 2022; Saber et al., 2021; Sahoo et al., 2023; Talukder et al., 2022; Mercaldo et al., 2023), VGG19 (Boudouh and Bouakkaz, 2023; Saber et al., 2021; Talukder et al., 2022; Lu

²⁰ <https://www.kaggle.com/datasets/ahmedhamada0/brain-tumor-detection>

²¹ <https://challenge.isic-archive.com/data>

²² <https://www.kaggle.com/c/siim-isic-melanoma-classification/overview>

²³ <https://dataverse.harvard.edu/dataset.xhtml?persistentId=doi:10.7910/DVN/DBW86T>

²⁴ <https://www.dermis.net/dermisroot/en/home/index.htm>

²⁵ <https://www.cancer.org/cancer/skin-cancer.html>

²⁶ <https://www.fc.up.pt/addi/ph2%20database.html>

²⁷ https://www.cs.rug.nl/~imaging/databases/melanoma_naevi/

et al., 2021; Shamim et al., 2022), ResNet50 (Teoh et al., 2024; Zeng et al., 2024; Sharmin et al., 2023; Boudouh and Bouakkaz, 2023; Asadi and Memon, 2023; Gonçalves et al., 2022; Alruwaili and Gouda, 2022; Saber et al., 2021; Haq et al., 2023; Deo et al., 2024; Shamim et al., 2022; Mercaldo et al., 2023), ResNet152, DenseNet121 (Fuentes-Fino et al., 2023; Dey et al., 2022; Paayas and Annamalai, 2023; Wei et al., 2020), DenseNet169 (Toma et al., 2023; Talukder et al., 2022; Marzouk et al., 2022), DenseNet201 (Gonçalves et al., 2022; Talukder et al., 2022; Noaman et al., 2024; Deo et al., 2024), InceptionV3 (Boudouh and Bouakkaz, 2023; Al Husaini et al., 2022; Saber et al., 2021; Shamim et al., 2022), Xception (Boudouh and Bouakkaz, 2023), ResNet101 (Boudouh and Bouakkaz, 2023), GoogleNet (Admass et al., 2024; Teoh et al., 2024; Sahoo et al., 2023; Lu et al., 2021; Shamim et al., 2022), AlexNet (Teoh et al., 2024; Boudouh and Bouakkaz, 2023; Fuentes-Fino et al., 2023; Lu et al., 2021; Shamim et al., 2022; Mercaldo et al., 2023), MobileNetV2 (Fuentes-Fino et al., 2023; Alqahtani et al., 2024; Wei et al., 2020; Mercaldo et al., 2023), YOLO (Anas et al., 2024), etc. The details are discussed in [Section 3.6](#).

RQ 3. a: The details of the research challenges and limitations are discussed in [Section 5.1](#).

RQ 3. b: The details of the future directions are discussed in [Section 5.2](#).

5.1. Challenges and limitations

5.1.1. Data quality and quantity

Imbalanced Datasets: Medical imaging datasets commonly display an imbalanced distribution of classes, with a higher prevalence of non-cancerous images compared to cancerous ones. This disproportion can result in biased models that inadequately address minority classes. In the context of lung cancer detection using CT scans, non-cancerous images frequently outnumber cancerous ones to a significant degree. This imbalance significantly impacts model training, leading to a notably high FNR. **Labeling Errors:** Accurate annotation of medical images is absolutely essential, but it presents a significant challenge due to inter-observer variability and the requirement for expert radiologists. Accurate annotation of microcalcifications and masses in breast cancer detection using mammograms demands the expertise of experienced radiologists. Any discrepancies between annotators can significantly impact model performance. **Limited Availability:** Access to substantial and diverse datasets is limited by privacy concerns and the proprietary nature of medical data. For instance, obtaining high-quality MRI scans for brain tumour detection is hindered by the high cost and privacy concerns, posing a significant challenge in compiling large datasets for training deep learning models.

5.1.2. Model generalization

Overfitting: Deep learning models, especially CNNs, are prone to overfitting, especially when they are trained on small or homogeneous datasets. For example, a deep learning model trained on a limited dataset of skin lesion images may achieve good performance on the training data but struggle to generalize to new images, leading to poor performance on unseen cases. **Domain Adaptation:** It's imperative to recognize that models trained on data from a particular institution or demographic are unlikely to perform optimally on data from another, which underscores the critical need for robust domain adaptation techniques. For example, a model trained to detect liver cancer using CT scans from one hospital will likely falter when dealing with CT scans from another hospital due to discrepancies in imaging protocols and patient demographics.

5.1.3. Complexities in segmentation

Variability in Tumor Appearance: Tumors can vary significantly in size, shape, and texture, making accurate segmentation challenging.

Example: In prostate cancer detection using MRI, tumours can vary greatly in size, shape, and contrast, making accurate segmentation challenging. **Boundary Delineation:** Precisely delineating tumour boundaries is difficult due to factors like image noise, low contrast, and the presence of artifacts. Example: Glioblastoma segmentation in brain MRIs is difficult due to the infiltrative nature of the tumour, which can blend with surrounding brain tissues, complicating boundary delineation.

5.1.4. Interpretability and trustworthiness

Black-Box Nature: While deep learning models have achieved high accuracy in cancer detection, segmentation, and classification, their lack of interpretability makes it challenging to understand the reasoning behind their predictions, which is crucial for clinical decision-making. Example: In colorectal cancer detection using colonoscopy images, the deep learning model's decision-making process can be opaque, making it difficult for clinicians to understand why certain polyps are classified as malignant. **Explainability:** Providing understandable explanations for model predictions is essential for clinical acceptance but remains a significant challenge. Example: For pancreatic cancer detection using CT scans, providing clear explanations for the model's predictions is crucial for gaining clinician trust and ensuring the model's integration into the diagnostic process.

5.1.5. Computational and infrastructure challenges

High Computational Costs: Training deep learning models on large medical imaging datasets requires substantial computational resources, including powerful GPUs and significant memory. Example: Training a deep learning model for whole-slide imaging in histopathology to detect breast cancer involves processing gigapixel images, requiring substantial computational resources. **Data Storage:** Medical imaging data, such as high-resolution scans, requires large storage capacities and efficient data management systems. Example: High-resolution PET scans for detecting metastasis in various cancers require large storage capacities, necessitating efficient data management solutions. **Integration with Existing Systems:** Integrating deep learning models into existing clinical workflows and electronic health record (EHR) systems is a complex task, requiring interoperability and seamless data exchange. Example: Integrating a deep learning model for prostate cancer detection into existing radiology workflows and EHR systems can be challenging, requiring significant efforts for interoperability and seamless data exchange.

5.2. Future directions

5.2.1. Development of robust and interpretable models

Hybrid Models: Combining deep learning with traditional machine learning and statistical methods to enhance interpretability. Example: Combining CNNs with traditional image processing techniques for better interpretability in detecting liver cancer from ultrasound images. **Explainable AI (XAI):** Investing in research to develop methods that provide clear, understandable explanations for model predictions. Example: Developing XAI methods to provide heatmaps highlighting regions of interest in mammograms for breast cancer detection, helping radiologists understand model predictions.

5.2.2. Enhancement of data availability and quality

Data Augmentation and Synthesis: Utilizing advanced data augmentation techniques and synthetic data generation to overcome data scarcity and imbalance. Example: Using GANs to create synthetic CT scans for lung cancer, improving model training by augmenting limited datasets. **Collaborative Data Sharing:** Encouraging collaborative efforts and frameworks for secure data sharing across institutions to build larger, more diverse datasets. Example: Establishing secure data-sharing frameworks across hospitals to build a larger, more diverse dataset for brain tumour detection using MRI.

5.2.3. Improving model generalization

Transfer Learning: Leveraging transfer learning to adapt pre-trained models to new datasets with limited labelled data. Example: Applying transfer learning from a pre-trained model on general medical images to improve performance in detecting skin cancer from dermoscopic images. **Domain Adaptation Techniques:** Developing advanced domain adaptation methods to ensure models perform well across different populations and imaging settings. Example: Developing domain adaptation methods to ensure a liver cancer detection model trained on one type of CT scanner generalizes well to images from different scanners.

5.2.4. Advanced segmentation techniques

Multi-Modal Imaging: Combining information from multiple imaging modalities (e.g., MRI, CT, PET) to improve segmentation accuracy. Example: Combining PET and CT scans for better segmentation of lung tumours, leveraging the complementary information from both modalities. **3D Segmentation:** Developing and refining 3D segmentation algorithms to better capture the spatial characteristics of tumours. Example: Developing 3D segmentation algorithms to capture the spatial characteristics of brain tumours from MRI, providing more accurate and comprehensive tumour delineation.

5.2.5. Integration into clinical practice

Clinical Trials and Validation: Conducting extensive clinical trials to validate the effectiveness and safety of deep learning models in real-world settings. Example: Conducting clinical trials to validate the effectiveness and safety of a deep learning model for colorectal cancer detection using colonoscopy videos in real-world settings.

5.2.6. Addressing ethical and privacy concerns

Federated Learning: Implementing federated learning approaches to train models on decentralized data without compromising patient privacy. Example: Implementing federated learning approaches to train models on decentralized breast cancer mammogram data from multiple institutions without compromising patient privacy. **Ethical Guidelines:** Establishing comprehensive ethical guidelines for the development and deployment of AI in medical imaging to ensure patient safety and data security. Example: Establishing ethical guidelines for the deployment of AI in detecting pancreatic cancer from CT scans, ensuring patient safety and data security.

6. Conclusion

The integration of deep learning algorithms into medical imaging for cancer detection, segmentation, and classification presents significant advancements in diagnostic accuracy, efficiency, and patient care. This survey highlights the notable successes in detecting various cancers, including lung, breast, prostate, brain, and skin cancers, while also identifying key research challenges and inherent limitations. Addressing issues such as data quality, model generalization, interpretability, and computational demands is essential for further progress. Future research should focus on developing robust, interpretable models, enhancing data availability, improving model generalization, and ensuring ethical and privacy considerations are met. By tackling these challenges and focusing on these future directions, the field can achieve more accurate, reliable, and clinically applicable solutions, ultimately revolutionizing cancer diagnosis and treatment and leading to better patient outcomes.

Conflict of Interest Statement

The authors declare that the research was conducted without any commercial or financial relationships that could be construed as a potential conflict of interest.

Author Contributions

Istiak Ahmad: Conceptualization, methodology, software, validation, formal analysis, investigation, resources, data curation, writing—original draft, visualization, funding acquisition. **Fahad Alqurashi:** Conceptualization, validation, formal analysis, investigation, resources, writing—review and editing, supervision, project administration. All authors have read and agreed to the published version of the manuscript.

Funding statement

The authors acknowledge with thanks the technical and financial support from the Deanship of Scientific Research (DSR) at the King Abdulaziz University (KAU), Jeddah, Saudi Arabia, under Grant No. (IFPIP: 1327-611-1443).

Declaration of Competing Interest

The authors declare that they have no known competing financial interests or personal relationships that could have appeared to influence the work reported in this paper.

References

- Abraham, B., Nair, M.S., 2018. Computer-aided classification of prostate cancer grade groups from mri images using texture features and stacked sparse autoencoder. *Comput. Med. Imaging Graph.* 69, 60–68.
- Admass, W.S., Munaye, Y.Y., Salau, A.O., 2024. Integration of feature enhancement technique in google inception network for breast cancer detection and classification. *J. Big Data* 11 (1), 78.
- Ahmad, I., AlQurashi, F., Abozinadah, E., Mehmood, R., 2021. A novel deep learning-based online proctoring system using face recognition, eye blinking, and object detection techniques. *Int. J. Adv. Comput. Sci. Appl.* 12 (10).
- Ahmad, I., Alqurashi, F., Abozinadah, E., Mehmood, R., 2022a. Deep journalism and deepjournal v1. 0: a data-driven deep learning approach to discover parameters for transportation. *Sustainability* 14 (9), 5711.
- I. Ahmad, F. AlQurashi, and R. Mehmood. Machine and deep learning methods with manual and automatic labelling for news classification in bangla language. arXiv preprint arXiv:2210.10903, 2022b.
- I. Ahmad, F. AlQurashi, and R. Mehmood. Potrika: Raw and balanced newspaper datasets in the bangla language with eight topics and five attributes. arXiv preprint arXiv: 2210.09389, 2022c.
- Al Husaini, M.A.S., Habaebi, M.H., Gunawan, T.S., Islam, M.R., Elsheikh, E.A.A., Suliman, F.M., 2022. Thermal-based early breast cancer detection using inception v3, inception v4 and modified inception mv4. *Neural Comput. Appl.* 34 (1), 333–348.
- Al-Dhabani, W., Gomaa, M., Khaled, H., Fahmy, A., 2020. Dataset of breast ultrasound images. *Data Brief.* 28, 104863.
- Al-Huseiny, M.S., Sajit, A.S., 2021. Transfer learning with googlenet for detection of lung cancer. *Indones. J. Electr. Eng. Comput. Sci.* 22 (2), 1078–1086.
- Alqahtani, H., Alabdulkreem, E., Alotaifai, F.A., Alnfiai, M.M., Singla, C., Salama, A.S., 2024. Improved water strider algorithm with convolutional autoencoder for lung and colon cancer detection on histopathological images. *IEEE Access* 12, 949–956.
- Alqarafi, A., Khan, A.A., Mahendran, R.K., Al-Sarem, M., Albalwy, F., 2024. Multi-scale gc-t2: Automated region of interest assisted skin cancer detection using multi-scale graph convolution and tri-movement based attention mechanism. *Biomed. Signal Process. Control* 95, 106313.
- Alqurashi, F., Ahmad, I., 2024. Scientometric analysis and knowledge mapping of cybersecurity. *Int. J. Adv. Comput. Sci. Appl.* 15 (3).
- Alruwaili, M., Gouda, W., 2022. Automated breast cancer detection models based on transfer learning. *Sensors* 22 (3), 876.
- Alzubaidi, M.A., Otoom, M., Jaradat, H., 2021. Comprehensive and comparative global and local feature extraction framework for lung cancer detection using ct scan images. *IEEE Access* 9, 158140–158154.
- Anas, M., Haq, I.U., Husnain, G., Faraz Jaffery, S.A., 2024. Advancing breast cancer detection: Enhancing yolov5 network for accurate classification in mammogram images. *IEEE Access* 12, 16474–16488.
- Ardakani, A.A., Mohammadi, A., Mirza-Aghazadeh-Attari, M., Acharya, U.R., 2023. An open-access breast lesion ultrasound image database: Applicable in artificial intelligence studies. *Comput. Biol. Med.* 152, 106438.
- Aresta, G., Aratijo, T., Kwok, S., Chennamsetty, S.S., Safwan, M., Alex, V., Marami, B., Prastawa, M., Chan, M., Donovan, M., et al., 2019. Bach: Grand challenge on breast cancer histology images. *Med. Image Anal.* 56, 122–139.
- Armato III, S.G., McLennan, G., Bidaut, L., McNitt-Gray, M.F., Meyer, C.R., Reeves, A.P., Zhao, B., Aberle, D.R., Henschke, C.I., Hoffman, E.A., et al., 2011. The lung image database consortium (lidc) and image database resource initiative (idri): a completed reference database of lung nodules on ct scans. *Med. Phys.* 38 (2), 915–931.

- Asadi, B., Memon, Q., 2023. Efficient breast cancer detection via cascade deep learning network. *Int. J. Intell. Netw.* 4, 46–52.
- Ashraf, R., Afzal, S., Rehman, A.U., Gul, S., Baber, J., Bakhtyar, M., Mehmood, I., Song, O.-Y., Maqsood, M., 2020. Region-of-interest based transfer learning assisted framework for skin cancer detection. *IEEE Access* 8, 147858–147871.
- Aygin, D., Yaman, O., 2022. Breast cancer in men: Risk factors, treatment options, quality of life: Systematic review. *Clin. Exp. Health Sci.* 12 (1), 257–267.
- Azevedo, V., Silva, C., Dutra, I., 2022. Quantum transfer learning for breast cancer detection. *Quantum Mach. Intell.* 4 (1), 5.
- Bashkanov, O., Rak, M., Meyer, A., Engelage, L., Lumiani, A., Muschter, R., Hansen, C., 2023. Automatic detection of prostate cancer grades and chronic prostatitis in biparametric mri. *Comput. Methods Prog. Biomed.* 239, 107624.
- Bhatt, A.R., Ganatra, A., Kotecha, K., 2021. Cervical cancer detection in pap smear whole slide images using convnet with transfer learning and progressive resizing. *PeerJ Comput. Sci.* 7, e348.
- Bhattacharjee, A., Murugan, R., Goel, T., 2022. A hybrid approach for lung cancer diagnosis using optimized random forest classification and k-means visualization algorithm. *Health Technol.* 12 (4), 787–800.
- Bilic, P., Christ, P., Li, H.B., Vorontsov, E., Ben-Cohen, A., Kaassis, G., Szeksin, A., Jacobs, C., Mamani, G.E.H., Chartrand, G., et al., 2023. The liver tumor segmentation benchmark (lits). *Med. Image Anal.* 84, 102680.
- Boudoul, S.S., Bouakkaz, M., 2023. Breast cancer: toward an accurate breast tumor detection model in mammography using transfer learning techniques. *Multimed. Tools Appl.* 82 (22), 34913–34936.
- Breast tumor facts. National Brain Tumor Society, (<https://braintumor.org/brain-tumor/s/about-brain-tumors/brain-tumor-facts/>).2024, Accessed: 05-07-2024.
- Bray, F., Laversanne, M., Sung, H., Ferlay, J., Siegel, R.L., Soerjomataram, I., Jemal, A., 2024. Global cancer statistics 2022: Globocan estimates of incidence and mortality worldwide for 36 cancers in 185 countries. *CA: a Cancer J. Clin.* 74 (3), 229–263.
- Breast cancer. World Health Organization, (<https://www.who.int/news-room/fact-sheets/detail/breast-cancer>), 2024. Accessed: 05-07-2024.
- Bulten, W., Kartasalo, K., Chen, P.-H.C., Ström, P., Pinckaers, H., Nagpal, K., Cai, Y., Steiner, D.F., Van Boven, H., Vink, R., et al., 2022. Artificial intelligence for diagnosis and gleason grading of prostate cancer: the panda challenge. *Nat. Med.* 28 (1), 154–163.
- Calderon-Ramirez, S., Murillo-Hernandez, D., Rojas-Salazar, K., Elizondo, D., Yang, S., Moemeni, A., Molina-Cabello, M., 2022. A real use case of semi-supervised learning for mammogram classification in a local clinic of costa rica. *Med. Biol. Eng. Comput.* 60 (4), 1159–1175.
- Cancer stat facts: Brain and other nervous system cancer. National Cancer Institute, (<https://seer.cancer.gov/statfacts/html/brain.html>).2024, Accessed: 05-07-2024.
- Cancer stat facts: Liver and intrahepatic bile duct cancer. National Cancer Institute, (<https://seer.cancer.gov/statfacts/html/livibd.html>).2024. Accessed: 05-07-2024.
- Cancer stat facts: Melanoma of the skin. National Cancer Institute, (<https://seer.cancer.gov/statfacts/html/melan.html>).2024, Accessed: 05-07-2024.
- Cancer stat facts: Pancreatic cancer. National Cancer Institute, (<https://seer.cancer.gov/statfacts/html/pancreas.html>).2024, Accessed: 05-07-2024.
- Cassidy, B., Kendrick, C., Brodzicki, A., Jaworek-Korjakowska, J., Yap, M.H., 2022. Analysis of the isic image datasets: Usage, benchmarks and recommendations. *Med. Image Anal.* 75, 102305.
- Cervical cancer. World Health Organization, (<https://www.who.int/news-room/fact-sheets/detail/cervical-cancer>), 2024. Accessed: 05-07-2024.
- Chen, C.-B., Wang, Y., Fu, X., Yang, H., 2023. Recurrence network analysis of histopathological images for the detection of invasive ductal carcinoma in breast cancer. *IEEE/ACM Trans. Comput. Biol. Bioinforma.* 20 (5), 3234–3244.
- Chenyang, L., Chan, S.-C., 2020. A joint detection and recognition approach to lung cancer diagnosis from ct images with label uncertainty. *IEEE Access* 8, 228905–228921.
- Chicco, D., Jurman, G., 2020. The advantages of the matthews correlation coefficient (mcc) over f1 score and accuracy in binary classification evaluation. *BMC Genom.* 21, 1–13.
- Chikkalingaiah, S., RaoHari Prasad, S.A.P., Ugggregowda, L.D., 2023. Classification techniques using gray level co-occurrence matrix features for the detection of lung cancer using computed tomography imaging. *Int. J. Electr. Comput. Eng.* (2088-8708) 13 (5).
- Chlebus, G., Schenk, A., Moltz, J.H., van Ginneken, B., Hahn, H.K., Meine, H., 2018. Automatic liver tumor segmentation in ct with fully convolutional neural networks and object-based postprocessing. *Sci. Rep.* 8 (1), 15497.
- Clark, K., Vendt, B., Smith, K., Freymann, J., Kirby, J., Koppel, P., Moore, S., Phillips, S., Maffit, D., Pringle, M., et al., 2013. The cancer imaging archive (tcia): maintaining and operating a public information repository. *J. Digit. Imaging* 26, 1045–1057.
- N.C.F. Codella, D. Gutman, M.E. Celebi, B. Helba, M.A. Marchetti, S.W. Dusza, A. Kalloo, K. Liopyris, N. Mishra, H. Kittler, et al. Skin lesion analysis toward melanoma detection: A challenge at the 2017 international symposium on biomedical imaging (isbi), hosted by the international skin imaging collaboration (isic).In: 2018 IEEE 15th international symposium on biomedical imaging (ISBI 2018), 168–172.IEEE, 2018.
- N. Codella, V. Rotemberg, P. Tschandl, M.E. Celebi, S. Dusza, D. Gutman, B. Helba, A. Kalloo, K. Liopyris, M. Marchetti, et al. Skin lesion analysis toward melanoma detection 2018: A challenge hosted by the international skin imaging collaboration (isic).arXiv preprint arXiv:1902.03368, 2019.
- Cohen, J., 1960. A coefficient of agreement for nominal scales. *Educ. Psychol. Meas.* 20 (1), 37–46.
- Colon cancer. World Health Organization, (<https://www.who.int/news-room/fact-sheets/detail/colorectal-cancer>), 2023. Accessed: 05-07-2024.
- Cruz-Orive, A., Basavanhally, A., González, F., Gilmore, H., Feldman, M., Ganesan, S., Shih, N., Tomaszewski, J., Madabhushi, A., 2014. Automatic detection of invasive ductal carcinoma in whole slide images with convolutional neural networks. volume 9041 Medical Imaging 2014: Digital Pathology. SPIE, 904103. volume 9041.
- de Vente, C., Vos, P., Hosseinzadeh, M., Pluim, J., Veta, M., 2021. Deep learning regression for prostate cancer detection and grading in bi-parametric mri. *IEEE Trans. Biomed. Eng.* 68 (2), 374–383.
- deo, B.S., Pal, M., Panigrahi, P.K., Pradhan, A., 2024. An ensemble deep learning model with empirical wavelet transform feature for oral cancer histopathological image classification. *Int. J. Data Sci. Anal.* 1–18.
- Devi, M.A., Sheeba, J.I., Joseph, K.S., 2022. Neutrosophic graph cut-based segmentation scheme for efficient cervical cancer detection. *J. King Saud. Univ. -Comput. Inf. Sci.* 34 (1), 1352–1360.
- Dey, S., Roychoudhury, R., Malakar, S., Sarkar, R., 2022. Screening of breast cancer from thermogram images by edge detection aided deep transfer learning model. *Multimed. Tools Appl.* 81 (7), 9331–9349.
- Dong, X., Zhou, Y., Wang, L., Peng, J., Lou, Y., Fan, Y., 2020. Liver cancer detection using hybridized fully convolutional neural network based on deep learning framework. *IEEE Access* 8, 129889–129898.
- A. Dosovitskiy, L. Beyer, A. Kolesnikov, D. Weissenborn, X. Zhai, T. Unterthiner, M. Dehghani, M. Minderer, G. Heigold, S. Gelly, et al. An image is worth 16x16 words: Transformers for image recognition at scale.arXiv preprint arXiv:2010.11929, 2020.
- Duran-Lopez, L., Dominguez-Morales, J.P., Conde-Martín, A.F., Vicente-Díaz, S., Linares-Barranco, A., 2020. Prometeo: A cnn-based computer-aided diagnosis system for wsi prostate cancer detection. *IEEE Access* 8, 128613–128628.
- Duran-Lopez, L., Dominguez-Morales, J.P., Gutierrez-Galan, D., Rios-Navarro, A., Jimenez-Fernandez, A., Vicente-Díaz, S., Linares-Barranco, A., 2021. Wide & deep neural network model for patch aggregation in cnn-based prostate cancer detection systems. *Comput. Biol. Med.* 136, 104743.
- Elakkiya, R., Subramanyaswamy, V., Vijayakumar, V., Mahanti, A., 2022. Cervical cancer diagnostics healthcare system using hybrid object detection adversarial networks. *IEEE J. Biomed. Health Inform.* 26 (4), 1464–1471.
- Esophageal cancer. National Cancer Institute, (<https://www.cancer.gov/types/esophageal>).2024 Accessed: 05-07-2024.
- Explore cancer statistics. American Cancer Society, (<https://cancerstatisticscenter.cancer.org/#/>), 2024. Accessed: 10-07-2024.
- Fahad, N.M., Azam, S., Montaha, S., Hossain Mukta, Md.S., 2024. Enhancing cervical cancer diagnosis with graph convolution network: Ai-powered segmentation, feature analysis, and classification for early detection. *Multimed. Tools Appl.* 1–25.
- Florimbi, G., Fabelo, H., Torti, E., Ortega, S., Marrero-Martin, M., Callico, G.M., Danese, G., Leporati, F., 2020. Towards real-time computing of intraoperative hyperspectral imaging for brain cancer detection using multi-gpu platforms. *IEEE Access* 8, 8485–8501.
- Fraiwan, M., Faouri, E., 2022. On the automatic detection and classification of skin cancer using deep transfer learning. *Sensors* 22 (13), 4963.
- Fuentes-Fino, R., Calderon-Ramirez, S., Dominguez, E., Lopez-Rubio, E., Elizondo, D., Molina-Cabello, M.A., 2023. An uncertainty estimator method based on the application of feature density to classify mammograms for breast cancer detection. *Neural Comput. Appl.* 35 (30), 22151–22161.
- Gade, A., Dash, D.K., Kumari, T.M., Ghosh, S.K., Tripathy, R.K., Pachori, R.B., 2023. Multiscale analysis domain interpretable deep neural network for detection of breast cancer using thermogram images. *IEEE Trans. Instrum. Meas.* 72, 1–13.
- R. Girshick.Fast r-cnn.In: Proceedings of the IEEE international conference on computer vision, 1440–1448, 2015.
- Gonçalves, C.B., Souza, J.R., Fernandes, H., 2022. Cnn architecture optimization using bio-inspired algorithms for breast cancer detection in infrared images. *Comput. Biol. Med.* 142, 105205.
- Goodfellow, I., Pouget-Abadie, J., Mirza, M., Xu, B., Warde-Farley, D., Ozair, S., Courville, A., Bengio, Y., 2020. Generative adversarial networks. *Commun. ACM* 63 (11), 139–144.
- D. Gutman, N.C.F. Codella, E. Celebi, B. Helba, M. Marchetti, N. Mishra, and A. Halpern. Skin lesion analysis toward melanoma detection: A challenge at the international symposium on biomedical imaging (isbi) 2016, hosted by the international skin imaging collaboration (isic).arXiv preprint arXiv:1605.01397, 2016.
- Hammouche, R., Attia, A., Akhrouf, S., Akhtar, Z., 2022. Gabor filter bank with deep autoencoder based face recognition system. *Expert Syst. Appl.* 197, 116743.
- Haq, I., Mazhar, T., Asif, R.N., Ghadi, Y.Y., Saleem, R., Mallek, F., Hamam, H., 2023. A deep learning approach for the detection and counting of colon cancer cells (ht-29 cells) bunches and impurities. *PeerJ Comput. Sci.* 9, e1651.
- Haron, N., Zain, R.B., Ramanathan, A., Abraham, M.T., Liew, C.S., Ng, K.G., Cheng, L.C., Husin, R.B., Chong, S.M.Y., Thangavalu, L.A.P., et al., 2020. m-health for early detection of oral cancer in low-and middle-income countries. *Telemed. e-Health* 26 (3), 278–285.
- K. He, G. Gkioxari, P., Dollár, and R. Girshick.Mask r-cnn.In: Proceedings of the IEEE international conference on computer vision, 2961–2969, 2017.
- Heath, M., Bowyer, K., Kopans, D., Kegelmeyer Jr, P., Moore, R., Chang, K., Munishkumar, S., 1998. Current status of the digital database for screening mammography. In: Digital Mammography: Nijmegen, 1998. Springer, pp. 457–460.
- hosseini, F., asadi, F., emami, H., ebnali, M., 2023. Machine learning applications for early detection of esophageal cancer: a systematic review. *BMC Med. Inform. Decis. Mak.* 23 (1), 124.

- A.G. Howard, M. Zhu, B. Chen, D. Kalenichenko, W. Wang, T. Weyand, M. Andreetto, and H. Adam. Mobilenets: Efficient convolutional neural networks for mobile vision applications. arXiv preprint arXiv:1704.04861, 2017.
- A. Howard, M. Sandler, G. Chu, L.-C. Chen, B. Chen, M. Tan, W. Wang, Y. Zhu, R. Pang, V. Vasudevan, et al. Searching for mobilenetv3. In: Proceedings of the IEEE/CVF international conference on computer vision, 1314-1324, 2019.
- Hu, Z., Tang, J., Wang, Z., Zhang, K., Zhang, L., Sun, Q., 2018. Deep learning for image-based cancer detection and diagnosis- a survey. *Pattern Recognit.* 83, 134–149.
- Haiping, J., Junlong, Z., Norouzzadeh Gil Molik, A.M., 2021. Skin cancer detection using kernel fuzzy c-means and improved neural network optimization algorithm. *Comput. Intell. Neurosci.* 1, 9651957.
- Hussain, S., Mubeen, I., Ullah, N., UdDinShah, S.S., Khan, B.A., Zahoor, M., Ullah, R., Khan, F.A., Sultan, M.A., 2022. Modern diagnostic imaging technique applications and risk factors in the medical field: a review. *BioMed. Res. Int.* 2022 (1), 5164970.
- Hussain, E., 2019. Liquid based cytology pap smear images for multi-class diagnosis of cervical cancer. *Data Brief.* 4.
- F. Iandola, M. Moskewicz, S. Karayev, R. Girshick, T. Darrell, and K. Keutzer. DenseNet: Implementing efficient convnet descriptor pyramids. arXiv preprint arXiv:1404.1869, 2014.
- Imran, A., Nasir, A., Bilal, M., Sun, G., Alzahrani, A., Almuhammed, A., 2022. Skin cancer detection using combined decision of deep learners. *ieee Access* 10 (october), 118198–118212.
- Iqbal, S., Siddiqui, G.F., Rehman, A., Hussain, L., Saba, T., Tariq, U., Abbasi, A.A., 2021. Prostate cancer detection using deep learning and traditional techniques. *IEEE Access* 9, 27085–27100.
- Jafari, Z., Karami, E., 2023. Breast cancer detection in mammography images: A cnn-based approach with feature selection. *Information* 14 (7), 410.
- Jain, D.K., Lakshmi, K.M., Varma, K.P., Ramachandran, M., Bharati, S., 2022. Lung cancer detection based on kernel pca-convolution neural network feature extraction and classification by fast deep belief neural network in disease management using multimedia data sources. *Comput. Intell. Neurosci.* 1, 3149406.
- Ji, M., Zhong, J., Xue, R., Su, W., Kong, Y., Fei, Y., Ma, J., Wang, Y., Mi, L., 2022. Early detection of cervical cancer by fluorescence lifetime imaging microscopy combined with unsupervised machine learning. *Int. J. Mol. Sci.* 23 (19), 11476.
- Kasban, H., El-Bendary, M.A.M., Salama, D.H., 2015. A comparative study of medical imaging techniques. *Int. J. Inf. Sci. Intell. Syst.* 4 (2), 37–58.
- Kashyap, R., 2023. Stochastic dilated residual ghost model for breast cancer detection. *J. Digit. Imaging* 36 (2), 562–573.
- Kaur, C., Garg, U., 2023. Artificial intelligence techniques for cancer detection in medical image processing: A review. *Mater. Today: Proc.* 81, 806–809.
- Kavitha, P., Ayyappan, G., Jayagopal, P., Mathivanan, S.K., Mallik, S., Al-Rasheed, A., Alqahtani, M.S., Souffiene, B.O., 2023. Detection for melanoma skin cancer through accf, bppf, and clf techniques with machine learning approach. *BMC Bioinforma.* 24 (1), 458.
- Khan, S., Nosheen, F., AliNaqvi, S.S., Jamil, H., Faseeh, M., AliKhan, M., Kim, D.-H., 2024. Bilevel hyperparameter optimization and neural architecture search for enhanced breast cancer detection in smart hospitals interconnected with decentralized federated learning environment. *IEEE Access* 12, 63618–63628.
- Krizhevsky, A., Sutskever, I., Hinton, G.E., 2017. Imagenet classification with deep convolutional neural networks. *Commun. ACM* 60 (6), 84–90.
- Kumar, Y., Gupta, S., Singla, R., Hu, Y.-C., 2022. A systematic review of artificial intelligence techniques in cancer prediction and diagnosis. *Arch. Comput. Methods Eng.* 29 (4), 2043–2070.
- Kumar, A., Singh, A.K., Singh, A., Kumar, V., Prakash, S., Tiwari, P.K., 2024. An efficient framework for brain cancer identification using deep learning. *Multimed. Tools Appl.* 1–30.
- Lee, R.S., Gimenez, F., Hoogi, A., Miyake, K.K., Gorovoy, M., Rubin, D.L., 2017. A curated mammography data set for use in computer-aided detection and diagnosis research. *Sci. data* 4 (1), 1–9.
- Li, X., Chen, H., Qi, X., Dou, Q., Fu, C.-W., Heng, P.-A., 2018. H-denseunet: hybrid densely connected unet for liver and tumor segmentation from ct volumes. *IEEE Trans. Med. Imaging* 37 (12), 2663–2674.
- Li, G., Li, C., Wu, G., Ji, D., Zhang, H., 2021a. Multi-view attention-guided multiple instance detection network for interpretable breast cancer histopathological image diagnosis. *IEEE Access* 9, 79671–79684.
- Li, Z., Li, Z., Chen, Q., Ramos, A., Zhang, J., Boudreault, J.P., Thiagarajan, R., Bren-Mattison, Y., Dunham, M.E., McWhorter, A.J., et al., 2021b. Detection of pancreatic cancer by convolutional-neural-network-assisted spontaneous raman spectroscopy with critical feature visualization. *Neural Netw.* 144, 455–464.
- Liberini, V., Pizzuto, D.A., Messerli, M., Orita, E., Grüning, H., Maurer, A., Mader, C., Husmann, L., Deandrea, D., Kotasidis, F., et al., 2022. Bsrem for brain metastasis detection with 18f-fdg-pet/ct in lung cancer patients. *J. Digit. Imaging* 35 (3), 581–593.
- Litjens, G., Debats, O., Barentsz, J., Karssemeijer, N., Huisman, H., 2014a. Computer-aided detection of prostate cancer in mri. *IEEE Trans. Med. Imaging* 33 (5), 1083–1092.
- Litjens, G., Toth, R., Van De Ven, W., Hoeks, C., Kerkstra, S., Van Ginneken, B., Vincent, G., Guillard, G., Birbeck, N., Zhang, J., et al., 2014b. Evaluation of prostate segmentation algorithms for mri: the promise12 challenge. *Med. Image Anal.* 18 (2), 359–373.
- Liver and bile duct cancer. National Cancer Institute, (<https://www.cancer.gov/types/liver>). 2024. Accessed: 05-07-2024.
- Lu, X., Nanehkaran, Y.A., Fard, M.K., 2021. A method for optimal detection of lung cancer based on deep learning optimized by marine predators algorithm. *Comput. Intell. Neurosci.* 2021 (1), 3694723.
- Lu, S.-Y., Wang, S.-H., Zhang, Y.-D., 2022. Safnet: A deep spatial attention network with classifier fusion for breast cancer detection. *Comput. Biol. Med.* 148, 105812.
- Lung cancer. World Health Organization, (<https://www.who.int/news-room/fact-sheet/s/detail/lung-cancer>), 2023. Accessed: 05-07-2024.
- Malik, H., Anees, T., Din, M., Naeem, A., 2023. Cdc_net: Multi-classification convolutional neural network model for detection of covid-19, pneumothorax, pneumonia, lung cancer, and tuberculosis using chest x-rays. *Multimed. Tools Appl.* 82 (9), 13855–13880.
- Marinakis, Y., Marinaki, M., Dounias, G., Jantzen, J., Bjerregaard, B., 2009a. Intelligent and nature inspired optimization methods in medicine: the pap smear cell classification problem. *Expert Syst.* 26 (5), 433–457.
- Marinakis, Y., Dounias, G., Jantzen, J., 2009b. Pap smear diagnosis using a hybrid intelligent scheme focusing on genetic algorithm based feature selection and nearest neighbor classification. *Comput. Biol. Med.* 39 (1), 69–78.
- Marzouk, R., Alabdulkreem, E., Dhahbi, S., Nour, M.K., Duhayyim, M.A., Othman, M., Hamza, M.A., Motwakel, A., Yaseen, I., Rizwanullah, M., 2022. Deep transfer learning driven oral cancer detection and classification model. *Comput. Mater. Contin.* 73 (2).
- Masood, A., Yang, P., Sheng, B., Li, H., Li, P., Qin, J., Lanfranchi, V., Kim, J., Feng, D.D., 2020a. Cloud-based automated clinical decision support system for detection and diagnosis of lung cancer in chest ct. *IEEE J. Transl. Eng. Health. Med.* 8, 1–13.
- Masood, A., Sheng, B., Yang, P., Li, P., Li, H., Kim, J., Feng, D.D., 2020b. Automated decision support system for lung cancer detection and classification via enhanced rfcn with multilayer fusion rpn. *IEEE Trans. Ind. Inform.* 16 (12), 7791–7801.
- Maurya, S., Tiwari, S., Mothukuri, M.C., Tangeda, C.M., Nandigam, R.N.S., Addagiri, D. C., 2023. A review on recent developments in cancer detection using machine learning and deep learning models. *Biomed. Signal Process. Control* 80, 104398.
- Mazrooa, A.A., Ishak, M.K., Aljarbouh, A., Mostafa, S.M., 2023. Improved bald eagle search optimization with deep learning-based cervical cancer detection and classification. *IEEE Access* 11, 135175–135184.
- McNeal, J.E., Redwine, E.A., Freiha, F.S., Stamey, T.A., 1988. Zonal distribution of prostatic adenocarcinoma: correlation with histologic pattern and direction of spread. *Am. J. Surg. Pathol.* 12 (12), 897–906.
- T. Mendonça, P.M. Ferreira, J.S. Marques, A.R.S. Marcal, and J. Rozeira. Ph2 - a dermoscopic image database for research and benchmarking. In: 2013 35th Annual International Conference of the IEEE Engineering in Medicine and Biology Society (EMBC), 5437-5440, 2013.
- Mercaldo, F., Brunese, L., Martinelli, F., Santone, A., Cesarelli, M., 2023. Explainable convolutional neural networks for brain cancer detection and localisation. *Sensors* 23 (17), 7614.
- Midasala, V.D., Prabhakar, B., Chaitanya, J.K., Sirinivas, K., Eshwar, D., Kumar, P.M., 2024. Mfeuslnet: Skin cancer detection and classification using integrated ai with multilevel feature extraction-based unsupervised learning. *Eng. Sci. Technol., Int. J.* 51, 101632.
- Mohakud, R., Dash, R., 2022. Designing a grey wolf optimization based hyper-parameter optimized convolutional neural network classifier for skin cancer detection. *J. King Saud. Univ. - Comput. Inf. Sci.* 34 (8), 6280–6291.
- Moreira, I.C., Amaral, I., Domingues, I., Cardoso, A., Cardoso, M.J., Cardoso, J.S., 2012. Inbreast: toward a full-field digital mammographic database. *Acad. Radiol.* 19 (2), 236–248.
- Mukhedkar, M., Rohatgi, D., Vuyyuru, V.A., Ramakrishna, K.V.S.S., Baker El-Ebary, Y. A., Asir Daniel, V.A., 2023. Feline wolf net: A hybrid lion-grey wolf optimization deep learning model for ovarian cancer detection. *Int. J. Adv. Comput. Sci. Appl.* 14 (9).
- Munir, K., Elahi, H., Ayub, A., Frezza, F., Rizzi, A., 2019. Cancer diagnosis using deep learning: a bibliographic review. *Cancers* 11 (9), 1235.
- Murthy, N.S., Bethala, C., 2023. Review paper on research direction towards cancer prediction and prognosis using machine learning and deep learning models. *J. Ambient. Intell. Humaniz. Comput.* 14 (5), 5595–5613.
- Myriam, H., Abdelhamid, A.A., El-Kenawy, E.-S.M., Ibrahim, A., Eid, M.M., Jamjoom, M. M., Khafaga, D.S., 2023. Advanced meta-heuristic algorithm based on particle swarm and al-biruni earth radius optimization methods for oral cancer detection. *IEEE Access* 11, 23681–23700.
- Naeem, A., Anees, T., Khalil, M., Zahra, K., Naqvi, R.A., Lee, S.-W., 2024. Snc_net: Skin cancer detection by integrating handcrafted and deep learning-based features using dermoscopy images. *Mathematics* 12 (7), 1030.
- NagaRamesh, J.V., Abirami, T., Gopalakrishnan, T., Narayanasamy, K., Ishak, M.K., Karim, F.K., Mostafa, S.M., Allakany, A., 2023. Sparrow search algorithm with stacked deep learning based medical image analysis for pancreatic cancer detection and classification. *IEEE Access* 11, 111927–111935.
- Nair, L.V., Jerome, S.A., 2024. Optimized pixel level image fusion for lung cancer detection over mri and pet image. *Multimed. Tools Appl.* 1–23.
- Nakano, K., Saito, Y., Kurabuchi, Y., Ohnishi, T., Ota, S., Uesato, M., Haneishi, H., 2020. Design of multiband switching illumination with low-concentration lugol stain for esophageal cancer detection. *IEEE Access* 8, 216043–216054.
- Napte, K.M., Mahajan, A., Urooj, S., 2023. Automatic liver cancer detection using deep convolution neural network. *IEEE Access* 11, 94852–94862.
- Nishio, M., Matsuo, H., Kurata, Y., Sugiyama, O., Fujimoto, K., 2023. Label distribution learning for automatic cancer grading of histopathological images of prostate cancer. *Cancers* 15 (5), 1535.
- Noaman, N.F., Kanber, B.M., Smadi, A.A., Jiao, L., Alsmadi, M.K., 2024. Advancing oncology diagnostics: Ai-enabled early detection of lung cancer through hybrid histological image analysis. *IEEE Access* 12, 64396–64415.
- Obayya, M., Arasi, M.A., Alruwais, N., Alsini, R., Mohamed, A., Yaseen, I., 2023. Biomedical image analysis for colon and lung cancer detection using tuna swarm algorithm with deep learning model. *IEEE Access* 11, 94705–94712.

- Oral cancer incidence (new cases) by age, race, and gender. National Institute of Dental and Craniofacial Research, (<https://www.nidcr.nih.gov/research/data-statistics/oral-cancer/incidence>).2024.Accessed: 05-07-2024.
- K. O'shea, R. Nash.An introduction to convolutional neural networks.arXiv preprint arXiv:1511.08458, 2015.
- Orthman, E., Mahmoud, M., Dhahri, H., Abdulkader, H., Mahmood, A., Ibrahim, M., 2022. Automatic detection of liver cancer using hybrid pre-trained models. *Sensors* 22 (14), 5429.
- Ovarian, fallopian tube, and primary peritoneal cancer. National Cancer Institute, (<https://www.cancer.gov/types/ovarian>).2024.Accessed: 06-07-2024.
- P. Paayas and R. Annamalai.Ocean - ovarian cancer subtype classification and outlier detection using densenet121.In: 2023 Seventh International Conference on Image Information Processing (ICIIP), 827-831, 2023.
- Park, J., Song, S., Kang, S.-H., Lee, Y., 2024. Performance evaluation of improved median-modified wiener filter with segmentation method to improve resolution in computed tomographic images. *J. Korean Phys. Soc.* 84 (7), 573-581.
- Pinckaers, H., Bulten, W., Van der Laak, J., Litjens, G., 2021. Detection of prostate cancer in whole-slide images through end-to-end training with image-level labels. *IEEE Trans. Med. Imaging* 40 (7), 1817-1826.
- Pirovano, A., Almeida, L.G., Ladjal, S., Bloch, I., Berlemont, S., 2021. Computer-aided diagnosis tool for cervical cancer screening with weakly supervised localization and detection of abnormalities using adaptable and explainable classifier. *Med. Image Anal.* 73, 102167.
- Plissiti, M.E., Dimitrakopoulos, P., Sfikas, G., Nikou, C., Krikoni, O., Charchanti, A., 2018. Sipakmed: A new dataset for feature and image based classification of normal and pathological cervical cells in pap smear images. 2018 25th IEEE international conference on image processing (ICIP). IEEE, pp. 3144-3148.
- Prabhu, S., Prasad, K., Robels-Kelly, A., Lu, X., 2022. Ai-based carcinoma detection and classification using histopathological images: A systematic review. *Comput. Biol. Med.* 142, 105209.
- Qian, Y., Zhang, Z., Wang, B., 2021. Procdet: A new method for prostate cancer detection based on mr images. *IEEE Access* 9, 143495-143505.
- Ragab, M.G., Abdulkadir, S.J., Muneer, A., Alqushaibi, A., Sumiea, E.H., Qureshi, R., Al-Selwi, S.M., Alhussian, H., 2024. A comprehensive systematic review of yolo for medical object detection (2018 to 2023). *IEEE Access* 12, 57815-57836.
- Rahman, T.Y., Mahanta, L.B., Das, A.K., Sarma, J.D., 2020. Histopathological imaging database for oral cancer analysis. *Data Brief* 29, 105114.
- Rai, H.M., 2024. Cancer detection and segmentation using machine learning and deep learning techniques: A review. *Multimed. Tools Appl.* 83 (9), 27001-27035.
- Rajagopalan, K., Babu, S., 2020. The detection of lung cancer using massive artificial neural network based on soft tissue technique. *BMC Med. Inform. Decis. Mak.* 20, 1-13.
- Ren, S., He, K., Girshick, R., Sun, J., 2015. Faster r-cnn: Towards real-time object detection with region proposal networks. *Adv. Neural Inf. Process. Syst.* 28.
- Ronneberger, O., Fischer, P., Brox, T., 2015. U-net: Convolutional networks for biomedical image segmentation. Medical image computing and computer-assisted intervention—MICCAI 2015: 18th international conference, Munich, Germany, October 5-9, 2015, proceedings, part III 18. Springer, pp. 234-241.
- Rotemberg, V., Kurtansky, N., Betz-Stablein, B., Caffery, L., Chousakos, E., Codella, N., Combalia, M., Dusza, S., Guitera, P., Gutman, D., et al., 2021. A patient-centric dataset of images and metadata for identifying melanomas using clinical context. *Sci. data* 8 (1), 34.
- Sánchez-Cauce, R., Pérez-Martín, J., Luque, M., 2021. Multi-input convolutional neural network for breast cancer detection using thermal images and clinical data. *Comput. Methods Prog. Biomed.* 204, 106045.
- Saber, A., Sakr, M., Abo-Seida, O.M., Keshk, A., Chen, H., 2021. A novel deep-learning model for automatic detection and classification of breast cancer using the transfer-learning technique. *IEEE Access* 9, 71194-71209.
- Sadad, T., Hussain, A., Munir, A., Habib, M., Khan, S.A., Hussain, S., Yang, S., Alawairdi, M., 2020. Identification of breast malignancy by marker-controlled watershed transformation and hybrid feature set for healthcare. *Appl. Sci.* 10 (6), 1900.
- Saha, A., Hosseiniyeh, M., Huisman, H., 2021. End-to-end prostate cancer detection in bpmri via 3d cnns: effects of attention mechanisms, clinical priori and decoupled false positive reduction. *Med. Image Anal.* 73, 102155.
- Sahoo, P., Saha, S., Mondal, S., Seera, M., Sharma, S.K., Kumar, M., 2023. Enhancing computer-aided cervical cancer detection using a novel fuzzy rank-based fusion. *IEEE Access* 11, 145281-145294.
- Sakr, A.S., Soliman, N.F., Al-Gaashani, M.S., Plawiak, P., Ateya, A.A., Hammad, M., 2022. An efficient deep learning approach for colon cancer detection. *Appl. Sci.* 12 (17), 8450.
- M. Sandler, A. Howard, M. Zhu, A. Zhmoginov, and L.-C. Chen.Mobilenetv2: Inverted residuals and linear bottlenecks.In: Proceedings of the IEEE conference on computer vision and pattern recognition, 4510-4520, 2018.
- Schwartz, D., Sawyer, T.W., Thurston, N., Barton, J., Ditzler, G., 2022. Ovarian cancer detection using optical coherence tomography and convolutional neural networks. *Neural Comput. Appl.* 34 (11), 8977-8987.
- Sedghi, A., Mehrtash, A., Jamzad, A., Amalou, A., Wells, W.M., Kapur, T., Kwak, J.T., Turkbey, B., Choyke, P., Pinto, P., et al., 2020. Improving detection of prostate cancer foci via information fusion of mri and temporal enhanced ultrasound. *Int. J. Comput. Assist. Radiol. Surg.* 15, 1215-1223.
- Sengupta, A., Ye, Y., Wang, R., Liu, C., Roy, K., 2019. Going deeper in spiking neural networks: Vgg and residual architectures. *Front. Neurosci.* 13, 95.
- Setio, A.A.A., Traverso, A., De Bel, T., Berens, M.S.N., Van Den Bogaard, C., Cerello, P., Chen, H., Dou, Q., Fantacci, M.E., Geurts, B., et al., 2017. Validation, comparison, and combination of algorithms for automatic detection of pulmonary nodules in computed tomography images: the luna16 challenge. *Med. Image Anal.* 42, 1-13.
- Shah, D., Khan, M.A.U., Abrar, M., Amin, F., Alkhamees, B.F., AlSalman, H., 2024. Enhancing the quality and authenticity of synthetic mammogram images for improved breast cancer detection. *IEEE Access* 12, 12189-12198.
- Shamim, M.Z.M., Syed, S., Shiblee, M., Usman, M., Ali, S.J., Hussein, H.S., Farrag, M., 2022. Automated detection of oral pre-cancerous tongue lesions using deep learning for early diagnosis of oral cavity cancer. *Comput. J.* 65 (1), 91-104.
- Sharma, P., Nayak, D.R., Balabantary, B.K., Tanveer, M., Nayak, R., 2023. A survey on cancer detection via convolutional neural networks: Current challenges and future directions. *Neural Netw.*
- Sharmin, S., Ahammad, T., Talukder, Md.A., Ghose, P., 2023. A hybrid dependable deep feature extraction and ensemble-based machine learning approach for breast cancer detection. *IEEE Access* 11, 87694-87708.
- Shiraishi, J., Katsuragawa, S., Ikezoe, J., Matsumoto, T., Kobayashi, T., Komatsu, K., Matsui, M., Fujita, H., Kodera, Y., Doi, K., 2000. Development of a digital image database for chest radiographs with and without a lung nodule: receiver operating characteristic analysis of radiologists' detection of pulmonary nodules. *Am. J. Roentgenol.* 174 (1), 71-74.
- Siegel, R.L., Giaquinto, A.N., Jemal, A., 2024. Cancer statistics, 2024. *CA: a Cancer J. Clin.* 74 (1), 12-49.
- Silva, L.F., Saade, D.C.M., Sequeiros, G.O., Silva, A.C., Paiva, A.C., Bravo, R.S., Conci, A., 2014. A N. Database Breast Res. *Infrared Image J. Med. Imaging Health Inform.* 4 (1), 92-100.
- Skin cancer. American Cancer Society, (<https://www.cancer.org/cancer/types/skin-cancer.html>).2024.Accessed: 05-07-2024.
- L. Soler, A. Hostettler, V. Agnus, A. Charnoz, J.-B. Fasquel, J. Moreau, A.-B. Osswald, M. Bouhadjar, and J. Marescaux.3d image reconstruction for comparison of algorithm database.(<https://www.ircad.fr/research/data-sets/liver-segmentation-3d-irca-db-01>), 2010.
- Spanhol, F.A., Oliveira, L.S., Petitjean, C., Heutte, L., 2015. A dataset for breast cancer histopathological image classification. *Ieee Trans. Biomed. Eng.* 63 (7), 1455-1462.
- Sriwastava, A., ArulJothi, J.A., 2024. Vision transformer and its variants for image classification in digital breast cancer histopathology: A comparative study. *Multimed. Tools Appl.* 83 (13), 39731-39753.
- Stabellini, N., Chandar, A.K., Chak, A., Barda, A.J., Dmukauskas, M., Waite, K., Barnholtz-Sloan, J.S., 2022. Sex differences in esophageal cancer overall and by histological subtype. *Sci. Rep.* 12 (1), 5248.
- Strelcenia, E., Prakoonwit, S., 2023. Improving cancer detection classification performance using gans in breast cancer data. *IEEE Access* 11, 71594-71615.
- Suckling, J., Parker, J., Dance, D., Astley, S., Hutt, I., and Boggis, C. Mammographic image analysis society (mias) database v1.21. University of Cambridge Repository, 2015.
- Sun, L., Ma, W., Ding, X., Huang, Y., Liang, D., Paisley, J., 2019a. A 3d spatially weighted network for segmentation of brain tissue from mri. *IEEE Trans. Med. Imaging* 39 (4), 898-909.
- Sun, L., Shao, W., Zhang, D., Liu, M., 2019b. Anatomical attention guided deep networks for roi segmentation of brain mr images. *IEEE Trans. Med. Imaging* 39 (6), 2000-2012.
- C. Szegedy, W. Liu, Y. Jia, P. Sermanet, S. Reed, D. Anguelov, D. Erhan, V. Vanhoucke, and A. Rabinovich.Going deeper with convolutions.In: Proceedings of the IEEE conference on computer vision and pattern recognition, 1-9, 2015.
- C. Szegedy, V. Vanhoucke, S. Ioffe, J. Shlens, and Z. Wojna.Rethinking the inception architecture for computer vision.In: Proceedings of the IEEE conference on computer vision and pattern recognition, 2818-2826, 2016.
- Talukder, M.A., Islam, M.M., Uddin, M.A., Akhter, A., Hasan, K.F., Moni, M.A., 2022. Machine learning-based lung and colon cancer detection using deep feature extraction and ensemble learning. *Expert Syst. Appl.* 205, 117695.
- Teoh, J.R., Hasikin, K., Lai, K.W., Wu, X., Li, C., 2024. Enhancing early breast cancer diagnosis through automated microcalcification detection using an optimized ensemble deep learning framework. *PeerJ Comput. Sci.* 10, e2082.
- Thanh, D.N.H., Prasath, V.B.S., Hieu, L.M., Hien, N.N., 2020. Melanoma skin cancer detection method based on adaptive principal curvature, colour normalisation and feature extraction with the abcd rule. *J. Digit. Imaging* 33 (3), 574-585.
- Tolkach, Y., Ovtcharov, V., Pryalukhin, A., Eich, M.-L., Gaisa, N.T., Braun, M., Radzhabov, A., Quaas, A., Hammerer, P., Dellmann, A., et al., 2023. An international multi-institutional validation study of the algorithm for prostate cancer detection and gleason grading. *NPJ Precis. Oncol.* 7 (1), 77.
- Toma, T.A., Biswas, S., Miah, M.S., Alibakhshikenari, M., Virdee, B.S., Fernando, S., Rahman, M.H., Ali, S.M., Arpanaei, F., Hossain, M.A., et al., 2023. Breast cancer detection based on simplified deep learning technique with histopathological image using breakhis database. *Radio Sci.* 58 (11), 1-18.
- Van Ginneken, B., Armato III, S.G., de Hoop, B., van Amelsvoort-van de Vorst, S., Duindam, T., Niemeijer, M., Murphy, K., Schilham, A., Retico, A., Fantacci, M.E., et al., 2010. Comparing and combining algorithms for computer-aided detection of pulmonary nodules in computed tomography scans: the anode09 study. *Med. Image Anal.* 14 (6), 707-722.
- Vaswani, A., Shazeer, N., Parmar, N., Uszkoreit, J., Jones, L., Gomez, A.N., Kaiser, L., Polosukhin, I., 2017. Attention is all you need. *Adv. Neural Inf. Process. Syst.* 30.
- Wang, S., Hamian, M., 2021. Skin cancer detection based on extreme learning machine and a developed version of thermal exchange optimization. *Comput. Intell. Neurosci.* 2021 (1), 9528664.
- Wang, Y., Wang, N., Xu, M., Yu, J., Qin, C., Luo, X., Yang, X., Wang, T., Li, A., Ni, D., 2020. Deeply-supervised networks with threshold loss for cancer detection in automated breast ultrasound. *IEEE Trans. Med. Imaging* 39 (4), 866-876.

- Wang, J., Qiao, L., Zhou, S., Zhou, J., Wang, J., Li, J., Ying, S., Chang, C., Shi, J., 2024. Weakly supervised lesion detection and diagnosis for breast cancers with partially annotated ultrasound images, 1-1 IEEE Trans. Med. Imaging, 1-1.
- Wei, L., Ding, K., Hu, H., 2020. Automatic skin cancer detection in dermoscopy images based on ensemble lightweight deep learning network. IEEE Access 8, 99633–99647.
- Welikala, R.A., Remagnino, P., Lim, J.H., Chan, C.S., Rajendran, S., Kallarakkal, T.G., Zain, R.B., Jayasinghe, R.D., Rimal, J., Kerr, A.R., et al., 2020. Automated detection and classification of oral lesions using deep learning for early detection of oral cancer. IEEE Access 8, 132677–132693.
- Wilson, P.F.R., Gilany, M., Jamzad, A., Fooladgar, F., Nhat To, M.N., Wodlinger, B., Abolmaesumi, P., Mousavi, P., 2023. Self-supervised learning with limited labeled data for prostate cancer detection in high-frequency ultrasound. IEEE Trans. Ultrason., Ferroelectr., Freq. Control 70 (9), 1073–1083.
- Xue, Y., Li, N., Wei, X., Wan, R.A., Wang, C., 2020. Deep learning-based earlier detection of esophageal cancer using improved empirical wavelet transform from endoscopic image. IEEE Access 8, 123765–123772.
- Yan, R., Ren, F., Wang, Z., Wang, L., Zhang, T., Liu, Y., Rao, X., Zheng, C., Zhang, F., 2020. Breast cancer histopathological image classification using a hybrid deep neural network. Methods 173, 52–60.
- Yan, Y.-J., Cheng, N.-L., Jan, C.-I., Tsai, M.-H., Chiou, J.-C., Ou-Yang, M., 2021. Band-selection of a portal led-induced autofluorescence multispectral imager to improve oral cancer detection. Sensors 21 (9), 3219.
- Yaqoob, A., Aziz, R.M., Verma, N.K., 2023a. Applications and techniques of machine learning in cancer classification: A systematic review. Hum. -Centr Intell. Syst. 3 (4), 588–615.
- Yaqoob, A., Aziz, R.M., Verma, N.K., Lalwani, P., Makrariya, A., Kumar, P., 2023b. A review on nature-inspired algorithms for cancer disease prediction and classification. Mathematics 11 (5), 1081.
- S. Zagoruyko and N. Komodakis. Wide residual networks. arXiv preprint arXiv: 1605.07146, 2016.
- Zeng, R., Qu, B., Liu, W., Li, J., Li, H., Bing, P., Duan, S., Zhu, L., 2024. Fastleakyresnet-cir: A novel deep learning framework for breast cancer detection and classification. IEEE Access 12, 70825–70832.
- Zheng, J., Lin, D., Gao, Z., Wang, S., He, M., Fan, J., 2020. Deep learning assisted efficient adaboost algorithm for breast cancer detection and early diagnosis. IEEE Access 8, 96946–96954.
- Zolfaghari, B., Mirsadeghi, L., Bibak, K., Kavousi, K., 2023. Cancer prognosis and diagnosis methods based on ensemble learning. ACM Comput. Surv. 55 (12), 1–34.